OCEAN SURFACE CURRENT ESTIMATION USING A LONG-RANGE, SINGLE-STATION, HIGH-FREQUENCY GROUND WAVE RADAR

KEN HICKEY

Ocean Surface Current Estimation Using a Long-Range, Single-Station, High-Frequency Ground Wave Radar

©Ken Hickey, B.Sc.

A THESIS SUBMITTED TO THE SCHOOL OF GRADUATE STUDIES IN PARTIAL FULFILLMENT OF THE REQUIREMENTS FOR THE DEGREE OF MASTER OF ENGINEERING

FACULTY OF ENGINEERING AND APPLIED SCIENCE
MEMORIAL UNIVERSITY OF NEWFOUNDLAND

MAY 1999

Abstract

Estimation of ocean surface currents from a long-range, single-station, narrow-beam, high frequency (HF) ground wave radar (GWR) system is presented. This system, located at Cape Race, Newfoundland, is a frequency modulated interrupted continuous wave radar that operates in the lower HF band between 5 and 8 Mhz. It has a nominal range capability of 200 km over a 120° sector from 61° to 181° (True). Even though its primary purpose is for offshore target surveillance, it can be easily configured for the monitoring of oceanic surface conditions such as currents and waves.

An experiment was performed during the fall of 1992 to test the current measuring capability of this experimental system. This HF GWR can monitor projections of the surface current field in azimuthal and range increments of approximately 4° and 400 m, respectively. These projections or radial surface current components are extracted from the first-order contributions of the radar Doppler spectra and compared with the estimates derived from the positional tracks of three Accurate Surface Tracker drifters. The comparison demonstrates the ability of the radar to estimate radial currents to within one standard deviation of both current measuring techniques. This has been demonstrated with simulated as well as actual data.

An algorithm is also presented to estimate the tangential current components assuming the current is uniform about the location of the drifter velocity estimate. This algorithm was tested with simulated radar data and the analysis suggests the error of the tangential component to be within one standard deviation of the radar and drifter error estimates. However, in the comparison using the real radar data these errors were more than 2 standard deviations larger than the errors estimated by the simulations. These deviations have been attributed to a number of factors such as possible beamforming errors or non-stationary currents over the radar beam dwell periods. However, since the simulations strongly demonstrate the potential for mapping the vector current field without the need of a second site, the results from this thesis are very encouraging for further development in this area.

In memory of my loving parents who passed away in March and April of 1995

May God bless them

Acknowledgements

Quite a number of individual efforts were required to make this small contribution to the engineering community possible.

I would first like to thank the local investment community who provided the funding to develop the Cape Race radar facility via Northern Radar Systems Limited. Without this backing, the work presented here would not be possible.

I would, secondly, like to thank the engineers who designed, built and managed the development of the radar system. These individuals include Dr. Rafaat Khan who designed the radar waveform and the signal processing chain, Bob Davis and Dr. Saoudy Saoudy who designed the antenna system, Fabian Hartery who painstakingly maintained it, Brian Gamberg and Wayne Pearson who wrote the system software, and Barry Dawe for his patient management of the project.

Dr. Jim Helbig of the Department of Fisheries and Oceans, who supervised the experiment and processed the drifter data, is gratefully acknowledged as well as the captain and crew of the HMCS Skeena who deployed the buoys.

I would also like to thank the system manager of Memorial's central computing facility, Randy Dodge, who gave me access to the VAX/VMS system for software development purposes. This was made increasingly difficult as this system, which contained all the processing software used to generate the early results from this thesis, was no longer being supported by the university during the period in early 1995 when the VAX/VMS system was being replaced by a UNIX platform.

Upon my departure from C-CORE in late 1995, the data and software from the VAX system was transferred to the computing facility at the engineering faculty. Therefore, I would like to thank Dave Press, the system manager of the Faculty of Engineering's computing facility, for helping me with the transition from the VAX/VMS platform to a UNIX system. This was a slow process since the file and software for-

mats had to be modified for access by the new system.

Upon my arrival at Raytheon Canada in 1996 the data files were reformatted again and further software re-writes were required. Therefore, I would like to thank Randy Howell of Raytheon Canada for helping to transfer all the radar data files to a Raytheon's PC environment and re-writing the Fortran code in MATLAB such that I could finish the data processing requirements for this thesis.

Eric Gill, who has taken the time to proofread and make suggestions regarding the presentation of this document, is also gratefully acknowledged. It was a pleasure to work with him over the past several years in this area since his enthusiastic approach to his research has provided me with much inspiration.

I also owe thanks to my partner and best friend, Rolanda Ryan. Her ability to know when and how to make me laugh during difficult periods in this academic endeavor is fondly appreciated. Her love and support were paramount to the completion of this work.

Finally, I would like to thankfully acknowledge my supervisor, Dr. John Walsh for his unwavering support over the past 10 years. In conjunction with Dr. Walsh, I would also like to thank the Faculty of Engineering for giving me the opportunity to undertake this task and enlighten myself and the HF radar community in the topic I have chosen as a thesis for my master's degree.

Contents

List of Figures

List of Tables

List of Symbols

d : Distance from radar sites to origin of two-station geometry

$\vec{V}$: Surface current vector

V_x : X component of surface current vector

V_y : Y component of surface current vector

$\vec{r_1}$: Unit vector along direction from radar site 1 to position of $\vec{V}$

$\vec{r_2}$: Unit vector along direction from radar site 2 to position of $\vec{V}$

V_1 : Projection of $\vec{V}$ along $\vec{r_1}$

V_2 : Projection of $\vec{V}$ along $\vec{r_2}$

L : Ocean wavelength

λ : Radar wavelength

V_b : Velocity of Bragg wave

g : Acceleration due to gravity

c : Speed of light

f_b : Bragg Doppler frequency

Δf : Dopper shift induced by currents

v_r : Radial component of current within a radar scattering cell

D : Length of linear array

f : Bandwidth of waveform transmitted by radar

Δt : Single beam dwell period

Δr : Effective radar range resolution

$\Delta \theta$: Effective radar receive beamwidth

$\mathbf{S}$: Region of uniform surface current

$\mathbf{Q}$: Polar sector which is a subset of region $\mathbf{S}$

$\hat{e}_j$: Unit vector along direction of centre of receive beam j

v_j : Radial component of $\vec{V}$ along $\hat{e}_j$

ΔR : Radial extent of region $\mathbf{Q}$

$\Delta\Theta$: Angular span of region $\mathbf{Q}$

m : Number of effective range cells comprising region $\mathbf{Q}$

n : Number of effective receive beams comprising region $\mathbf{Q}$

Θ_j : Angle of unit vector $\hat{e}_j$

$\hat{x}, \hat{y}$: Unit vector along x- and y-axes, respectively

v_{ij} : Radial current component in i^{th} and j^{th} effective range cell and receive beam, respectively, of region $\mathbf{Q}$

$\vec{v}$: Vector of all radial current projections within region $\mathbf{Q}$

$\vec{e}$: Vector of all error terms in $\vec{v}$

$\vec{\Phi_1}$: Vector of *cosines* of beam direction angles within region $\mathbf{Q}$

$\vec{\Phi_2}$: Vector of *sines* of beam direction angles within region $\mathbf{Q}$

F : Frequency range in Doppler spectrum used for computing signal noise floor

Chapter 1

Introduction

The monitoring of ocean surface currents is an important coastal management problem in the areas of offshore oil development, fisheries research and coastguard applications. Oil spill trajectories from tankers and offshore fields are largely determined by the motion of the surface layer. The transport of nutrients and fish larvae require knowledge of water movement for fisheries preservation research. Timely and accurate surface current data is also required for search and rescue models to optimize the size of search region zones when tracking drifting vessels. However, the surface current measurements obtained by conventional devices such as current meters and drifters may not give the required spatial or temporal detail to be optimal for the above purposes. In addition, the logistics associated with deploying these devices is difficult, time consuming and very expensive.

An alternative to these *in situ* techniques is provided by High Frequency (HF) radar using the ground wave mode of propagation. The HF band ranges from about 3 to 30 MHz, and at these frequencies the relatively high conductivity of the sea water enables the radar transmission to extend well beyond the line-of-sight range experienced by traditional microwave sensors. Because of the HF band's dekametric wavelengths, the dominant interaction is with the energy carrying long-wavelength gravity waves. These waves are usually of concern to offshore developers for structural design purposes. However, the analysis of backscattered radio waves from these ocean

waves is also useful for the estimation of surface layer physical oceanography and, in particular, surface currents.

Scattering of electromagnetic waves from rough surfaces is a classical problem in radio science, and the scattering of surface or ground waves from the sea is a special case. If ones assumes that the ocean surface can be represented by a three-dimensional Fourier transform, then the scattered wave energy can be modelled. Using this approach, the theory of ground wave radar, from an oceanographic perspective, has been well established. Barrick [1] formulated the first and second order radar cross-sections of the ocean surface. More recently, Walsh and Donnelly [2] have addressed fundamental electromagnetic scattering and propagation problems relating to HF ground wave radar (GWR) operation in an ocean environment. The latter work has led to the development of new radar cross-sections of the ocean surface to third order (Walsh *et al.* [3]). These efforts have provided the basis for the furtherance of GWR technology and have led to significant advances in the use of HF Doppler radars for the remote sensing of various oceanic surface parameters. In particular, narrow- and broad-beam arrays, operating in the ground wave mode, have been successfully employed in the determination of ocean currents, surface winds, and directional and nondirectional wave parameters (Hickey and Khan [4], Howell and Walsh [5], Gill and Walsh [6]). Such initiatives have been spurred on by the the fact that HF radars, as compared to *in situ* devices such as current meters or wave buoys, are able to provide comprehensive synoptic oceanographic information over a very large area.

HF radar surface current measurements are representative of the total current (i.e. the interactive sum of geostropic, tidal, wave, and wind generated components). All HF radars indirectly measure the component of the average current lying along the radar line of sight. For example, if the radar is directed at a patch of the ocean surface, it will observe the component of the surface current along the direction of observation. This is illustrated in Figure 1.1 where a uniform current is flowing

southward. In this example the same current projects different components along the three radar beam directions. These components or projections are referred to as the radial components of the surface current. By varying the operating frequency of the radar, the mean current for a variable depth may also be determined (Barrick *et al.* [7], Stewart and Joy [8]). If two or more radars map the radial current field from their common coverage areas, the vector surface current field can be estimated.

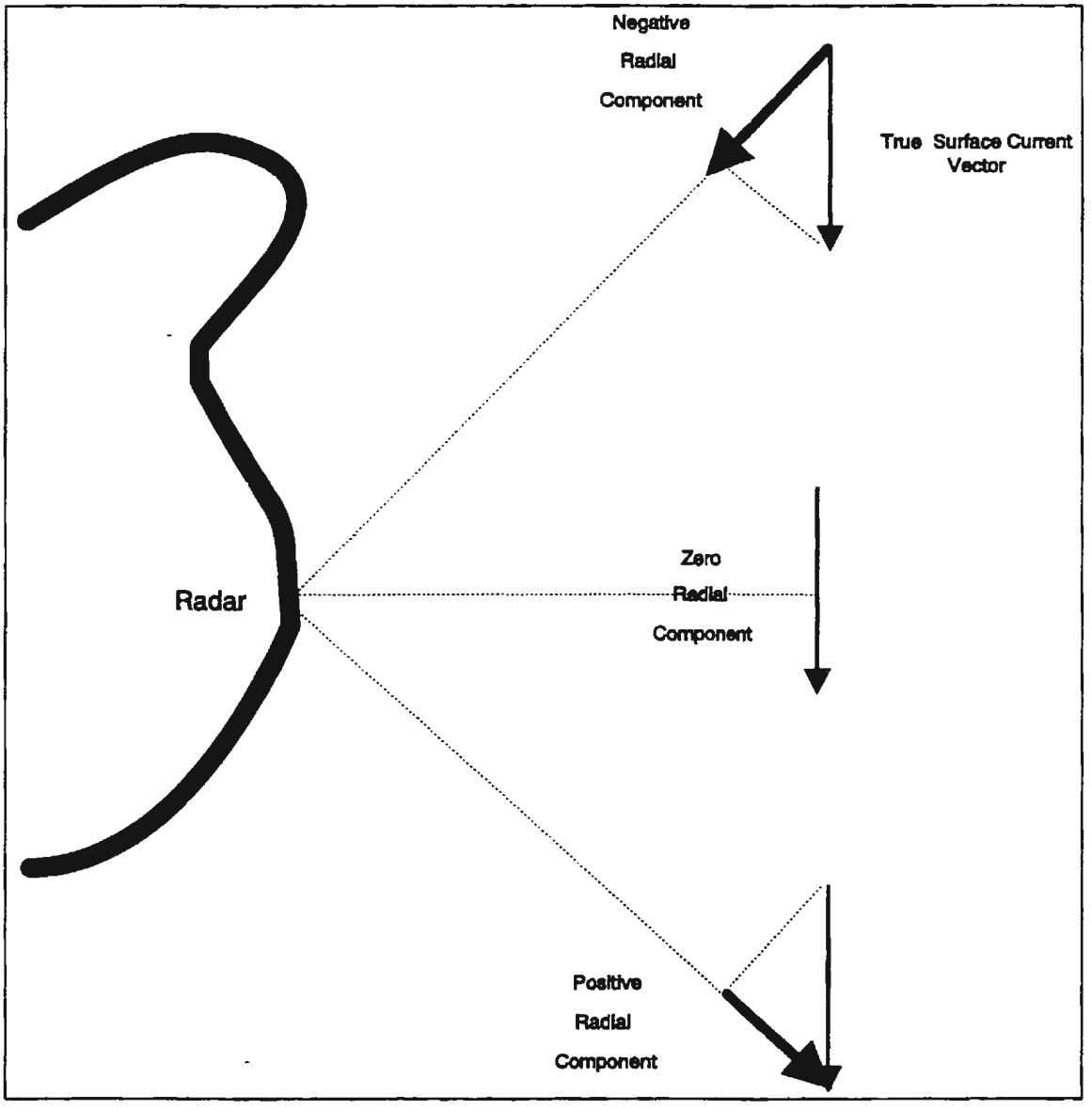

Figure 1.1: Radial component of true vector current as monitored by the radar along three different directions

1.1 Importance of Surface Currents

Besides waves, of all the oceanographic parameters that may affect offshore operations, currents are by far the most important (Hodgins [9]). The total flow at a particular position can be regarded as the superposition of current components from different forcing mechanisms. These currents are highly variable. Besides being driven by geostropic forces and tides, they are strongly influenced by the local surface wind and wave fields.

Currents near the surface are those which are associated with the mixed layer of the ocean. On the Grand Banks region off Newfoundland, for example, this layer ranges in depth from 25 to 100 metres below the ocean surface. Since currents in this layer are responsible for the transportation of any materials in the layer, being able to measure them is of great importance in the management of coastal areas. The following are a few examples of the use of this type of information.

- Tracking of oil and other surface-borne pollutants may be more easily performed.
- The data can be used by real-time ice and iceberg drift prediction models.
- Search and rescue teams can use the data to estimate the trajectory of a drifting vessel.
- The safe transfer of people and equipment at sea should be performed when surface current conditions are ideal, such as when net current flows are small.
- A knowledge of local surface current velocities is essential for the safe mooring of floating structures.
- Predictive models for extreme currents rely on long-term time series measurements. A database for these measurements, both spatially and temporally , can now be developed.

1.2 Conventional Methods for Measuring Currents

Fixed point estimates of the surface current have usually been performed by moored current meters (Beardsley *et al.* [10], Halpern [11], Weller and Davis [12]). Since these devices must be moored at depths exceeding 20 metres, they provide little indication of the current at the surface. Also, because of energetic high-frequency motions in the surface layers, data produced by these current meters are subject to various forms of contamination depending on the type of instrument, the mooring configuration and the type of environmental conditions experienced (Smith [13]).

Large-scale current circulation has conventionally been measured by the tracking of floating objects. Drogued or undrogued drifters are designed to follow the water such that they are only minimally influenced by wind. Since these drifters are tracked by aircraft, radar, vessels or satellite, using this technique to determine the surface current field can be quite expensive and very time-consuming (Diemand *et al.* [14],Petrie and Isenor [15]). Moreover, the spatial distribution of drifters changes with time as they pass through the region of interest and/or avoid areas of net divergence. This is important, for example, in fisheries applications for the understanding of plankton transport.

1.3 The HF Radar Technique

Crombie [26] deduced experimentally that the current beneath the surface waves of a patch of ocean could be measured indirectly by spectrally analysing the returned radar signal from that region. This was later confirmed, theoretically, by Barrick [1] and since Crombie's initial investigations, good quality measurments of surface currents have been obtained in North America, Europe and Australia using two station systems (Lipa and Barrick [17], Prandle and Ryder [18], Janopaul *et al.* [19]).

1.3.1 Advantages

There are numerous advantages in using HF radar technology for current measurement. Many of these are attributed to the unique allweather capability provided by the technology for long-term synoptic current mapping. The following advantages are especially noteworthy.

- Measurement of currents near the ocean surface is difficult using conventional systems and the formation of fine-resolution current maps has been virtually impossible. HF radar techniques overcome these difficulties when two stations are used to survey their common coverage areas.

- Extraction of current patterns using conventional methods cannot be performed in near real-time. Therefore, these methods are not useful for any real-time response such as would be desired in the implementation of oil-spill countermeasures.

- A database of surface currents can now be constructed to provide a better understanding of circulation patterns in regions of exploration and development, with a goal to ultimately understand how operations may be affected in these regions.

- Management requirements are dramatically reduced, as the overhead associated with conventional methods is eliminated by virtue of the fact that the currents are remotely sensed from a land-based station far removed from the region of interest.

- The prospect of having continuous surface current data should provide the impetus to correlate currents with their short-term driving forces such as winds, waves and tides. Potentially, such a correlation could be a means of using this data to measure those driving forces indirectly. Since these forces affect ice and

iceberg motion, a better relationship between currents and their effects can be obtained (Dinsmore [20]).

- Icebergs, bergy bits, and growlers may attain high velocities under the influence of surface currents. Therefore, detailed current records of the Grand Banks area, for example, may aid in the design of any platformed structures that may reside in the region.

- Real-time surface current records can aid in the prediction of the behaviour of ice over short time intervals. Even though the general drift of ice over a few days can be reasonably well defined, its short term response may not be.

Since the use of HF radar technology allows surface currents to be mapped over large spatial and temporal extents, it is clear that this technology offers superior and more economically feasible capabilities than conventional *in situ* devices.

1.3.2 Two Station Method

Ocean surface currents have been mapped by HF radar since the 1970's using short range (less than 60 km) broad-beam and narrow-beam systems. However, these short range systems were designed to measure near-shore currents which are generally of a more complex nature than their offshore equivalents. These systems consist of two spatially separated radars, where each records the radial component of the surface current field over a common coverage area. Data from one station is transferred to the other site for current map synthesis, where the vector or total current map is constructed from strictly geometric considerations. For example, consider Figure 1.2 where the x-axis of the co-ordinate system coincides with the line connecting the two sites and the origin is equi-distant from both stations. At the point (x,y), both radars measure the radial components or orthogonal projections of the current $\vec{\mathbf{V}}$. A direct sum of the components to yield the current vector is not possible since the

projections are not from an orthogonal reference frame. However, it can be shown that $\vec{\mathbf{V}}$ can be obtained from the following transformation

$$\begin{aligned} V_x &= \frac{r_2 \mathbf{V}_2 - r_1 \mathbf{V}_1}{2d} \\ V_y &= \frac{r_1 \mathbf{V}_1 (x+d) - r_2 \mathbf{V}_2 (x-d)}{2yd} \end{aligned} \tag{1.1}$$

where d is the distance from the origin to either site while r_1 and r_2 are the distances from (x,y) to both sites, respectively. This equation converts the two-site radial data ($\mathbf{V}_1$,$\mathbf{V}_2$) into a Cartesian vector (V_x,V_y). It may be noted from this transformation

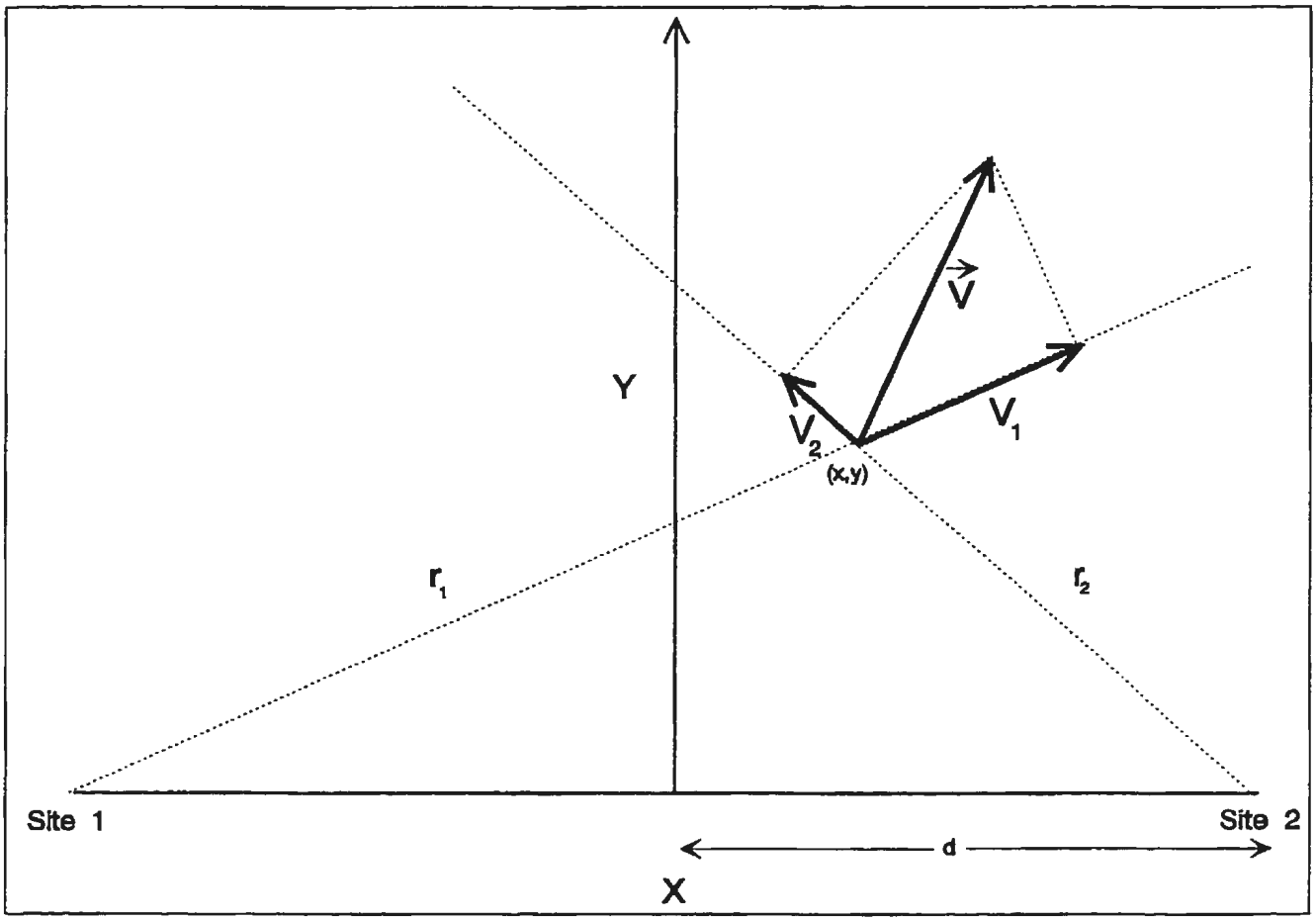

Figure 1.2: Geometry for two-station technique

that if y is small or x is large, the determination of V_y becomes unstable. Along the line between the two radar stations which is referred to as the baseline, the

magnitude of the radial component is the same from both sites. This is commonly referred to as the baseline instability. Also, at ranges which are much larger than the site separation, the same radial component is sensed from both sites. Therefore, the spacing of these stations must be determined from the single station range and the required coverage. However, if a two-station setup is logistically difficult to deploy an alternative approach may be needed.

1.3.3 One Station Approach

If the surface current field can be estimated using only one station, then the problems associated with the two-station approach can be avoided. First of all, the geometric constraints no longer apply since there are no baseline or range dependent instabilities. Also, hardware costs and manpower demands are minimized. Inter-site communication is also not necessary. This is especially useful in regions where only one site can be constructed due to geographic constraints.

The surface current vector estimated from the radial data is based on the assumption of a uniform current about the region where a point estimate is required. If this is the case the radial components within this region will simply be different projections of this current. By fitting the data in a least-squares sense we can obtain the original vector current. The quality of the fit can be determined by analysing the variance of the errors from the estimated and actual projections. For example, if the standard error is small as compared to the computed current magnitude, then the vector current is more likely to be uniform in the region. As well, an average current estimate may also be obtained if detailed current information is not required, for example in the estimation of the mean current vector over a large area for mesoscale current studies. However, this is dependent on the required application.

1.4 Literature Review

The origin of surface current measurements using HF radar can be traced to Crombie [16] when he analysed the Doppler frequency shift of a 13.56 MHz radio transmission which was reflected from the ocean surface. He observed a large peak in the radar spectra at 0.38 Hz. His explanation of this phenomena was that the sea waves act as diffraction gratings and "Bragg scatter" is observed. This is the same phenomenon which is responsible for the scattering of X-rays in crystals and light rays from holograms. Under given wind conditions, ocean waves of varying lengths are generated. Of these waves, those which have a wavelength L and are travelling to and away from the transmitter will reflect back a constructive signal when $L = \lambda/2$ where λ is the radar wavelength. Since we know the velocity of the sea wave, the Doppler shift of this enhanced signal can be easily computed. From Crombie's calculations he determined the Doppler frequency to be approximately 0.37 Hz, which was in close agreement with his experimental result.

The theory explaining Crombie's observations was not developed until some years later. Wait [21] observed that since the amplitude of the scattered signal is quite large, the reflection or scattering coefficient of the sea must be large as well. He, Wait [22], described a simple but quantitative theory for the resonant type of reflections which are seen in the Doppler spectra at HF by considering the ocean surface as "gently rippled". In this treatment, he considers a formulation for the signal received from an ocean patch which has been irradiated with energy from a vertical electric dipole when the antenna is transmitting pulses. From his result it is evident that the most significant response occurs when the radar wavelength is twice the wavelength of the ocean waves which are assumed to be responsible for the scatter. This is in agreement with Crombie's hypothesis in 1955 [16].

The problem of first-order HF radio wave scattering from a moving target such as the sea surface was addressed by Barrick [1]. Based on work by Peake [23] and

Rice [24], Barrick [1] developed an expression for the average backscattered signal power density spectrum. This expression, when integrated with respect to frequency, clearly shows that the ocean surface produces scatter by the Bragg mechanism, thus supporting Crombie's hypothesis in 1955[16] and Wait's formulation [22].

Since HF reflections from the sea surface are scattered constructively from ocean wavelengths, proportional to the radar wavelength, it was envisioned by Crombie that a multi-frequency HF system could be used as a sea-wave spectrometer. That is, the amplitudes of the dominant spectral components may be related to the waveheight of the gravity waves whose wavelengths interact constructively with the radar wave. In the 1960's, experiments were performed at Elgin Air Force Base on the Florida coast where an ionspheric sounder, modified to radiate in the horizontal direction, was used to collect the sea echo reflections in the 2 to 10 MHz band. The intent of these experiments was to compare the theoretical and measured Doppler shifts over the lower HF band (Crombie [25]). However, there were discrepancies between the simple theory that Crombie proposed in 1955 and the actual measurements. The first-order spectral components were slightly shifted from their theoretical values, which resulted in a velocity discrepancy of approximately 40 cm/s. Since this was comparable with the historical magnitudes of the ocean surface currents off the Florida coast, he surmised that ocean surface currents, induced by waves, winds and tides, accounted for this shift. That is, the whole water surface moves due to underlying currents.

Another experiment was performed at Jupiter Inlet, Florida, which utilized two spaced receiving antennae for direction-finding purposes to determine the directions in which the sea waves were travelling. By considering the coherence function of the signals received at the two antennae, Crombie [26] showed that constructive backscatter signals were received over a wide range of azimuths and their Doppler shifts indicated that the current was flowing nearly perpendicular to the coast and in the same direction as the wind.

Further experiments were conducted at a HF facility on San Clemente Island during the early 1970's to monitor currents. This installation used a phased-array to generate a narrow beam of approximately 15° along two seaward directions. During one experiment the current flow observed by the radar was consistent with the wind conditions, in that the current was approximately 3.5% of the wind speed (Wu [27]). A heuristic approach was used to explain the radar measured component of the current (Barrick *et al.* [7]). In another experiment drifting buoys, which could monitor the current at varying depths, were used to compare the radar and drifter-induced currents (Stewart and Joy [8]). These experiments strongly suggested the HF technique was a valid means of measuring ocean surface currents.

In 1975 , NOAA's Wave Propagation Laboratory developed a HF short range system called the Coastal Ocean Dynamics Applications Radar (CODAR). This system could monitor surface currents, to a range of 70 km, from two shored-based stations separated by approximately 20 km. Each station could measure the radial component of the surface current field of their common coverage areas. Hence, the vector component could be constructed from geometric considerations. CODAR operation was based on Crombie's two-element interferometer system in that a small aperture antenna using a direction-finding technique, developed by Munk *et al.* in 1963 [28], was used to resolve the direction of a signal over 360° with a four-element square array. Since this small aperture system was compact and portable the real estate requirements, which are needed to form a narrow beam using a linear phased array, were not necessary. These systems were used in over 20 experiments by NOAA and other agencies in order to verify the technique. Results of these investigations report maximum magnitude and directional errors of 15 cm/s and 10°, respectively. A sample of these investigations can be found in Holbrook and Frisch [29], Janopaul *et al.* [19], Lawrence and Smith [30] and Hodgins [31]. Other groups in Europe and Australia also verified the HF radar technique using a combination of short and long

range broad and narrow-beam systems (Collar *et al.* [32], Venn *et al.* [33], Essen *et al.* [34], Prandle [35], Heron *et al.* [36]).

This aforementioned HF technology was transferred to Canada in the early 1980's as part of a test-bed program to study the feasibility of using HF radar for the over-the-horizon detection of ice (Butt *et al.* [37], Butt and Hickey [38]). The research was initiated by Dr. John Walsh of The Faculty of Engineering at Memorial University of Newfoundland (MUN) and was comprised not only of ice detection research, but also research in the detection of ships, low-flying aircraft, and oceanographic surface parameter phenomenon such as currents and waves. The first use of this new technology for the purpose of current surveillance in Canada was in the winter of 1983. Two stations, one situated at Cappahayden, Newfoundland (NF), and the other at Cape Race, NF, were used to collect HF radar data from the ice-infested waters off the Ballard Bank. The successful initial trial was the first instance whereby current maps were obtained from radar data that was contaminated by sea ice reflections (Butt *et al.* [37]). Many more successful trials followed and the system was continually upgraded throughout the 1980's to help validate Walsh's models, via ice, ship, wave, and current trials, using various narrow- and broad-beam receiving antenna configurations (Walsh *et al.* [39], Gill and Walsh [6], Walsh and Srivastava [40]).

In the late 1980's the research effort in this area, at MUN, was at a mature stage. A local company, Northern Radar Systems Limited (NRSL), was formed to commercialize the results from the previous ten years of research. The first project for this new company was the complete construction of a multi-purpose, long range, shore based ground wave radar system at Cape Race, NF. This steerable narrow-beam system was designed to provide continuous surveillance of a 120° sector of ocean encompassing the greater Grand Banks, including the Hibernia and Terra Nova oil fields, out to a maximum range of 400 km.

One of the intended data products from this new long-range system is the produc-

tion of current maps. However, it is necessary to demonstrate that a single *long-range* station can provide adequate radial current estimates. One of the goals of this thesis is to report on this capability, since experimental results from such an exercise are not documented in the literature. As well, the new drifters used in the experiment are minimally influenced by wind, which has affected other past radar/drifter comparisons using short-range broad-beam systems. Therefore, a unique opportunity is now available to present a more realistic comparison between the current components from both techniques.

Two-station vector current mapping is also plausible provided other stations are built which are strategically located to share a common coverage zone. The successful demonstration of this capability would permit the radar to map the total current vector field. For example, the data from Cape Race could be coupled with data from a system at Cape Bonavista to routinely map the currents on the Grand Banks. This region, which is already known as one of the world's best fishing grounds, is now being developed because of its rich oil reserves. Reliable and timely surface current data is certainly useful for further offshore development planning. However, surface current data in this region is sparce and has typically been confined to current meter records at points of drilling activity. Since there are no detailed current records from this area, the radar data would provide valuable information in the study of the physical oceanography of the surface layer of the Grand Banks. This is even more compelling considering the recent collapse of the cod stocks and the apparent lack of understanding of the relationship of currents to this problem.

Since two stations are normally required to estimate vector currents, the facility at Cape Race provides an opportunity to test the feasibility of using a single-station, long-range radar to remotely estimate the total current field. This has not been documented in the literature for a long-range system. Investigations in this area have been confined only to one short-range system (Lipa and Barrick [17]). However,

the short-range radar is quite different from the Cape Race facility in that it uses a crossed-loop antenna system for broad-beam reception. Lipa and Barrick [17] formulated an expression for the radial current components as a linear function of the current magnitude and a non-linear function of direction. To solve these functions, a closed-form solution is used to estimate the current magnitude while the non-linear portion of the formulation is linearized and treated to a least squares solution. Errors using this formulation were found to range from 4 to 20 cm/s in magnitude and 12° to 30° in angle. However, there was no sea truthing for the results presented and consequently the above error statements could not be validated.

Another technique using a single station radar for vector current estimation is the spaced antenna (SA) technique which has been used for atmospheric radars in the determination of wind velocities since 1950 (Briggs *et al.* [41]). In 1989, this method was applied to a single-station short-range, narrow-beam, HF system for current measurements (May [42]). In that method, it can be shown that the backscattered electric field is translated across the receiving antenna system at a velocity of $2V$ where V is the tangential current velocity in the scattering area. Therefore, the cross-correlation function of the signal detected by two antenna separated by a distance d will have a peak at a time lag of $d/2V$. This technique could not be implemented using the experimental data in this thesis because the raw data was irreversibly processed to yield radial current maps. However, the radar could be configured to test such a technique by processing the baseband signal in the above manner. For this case, the original linear array would need to be partitioned into two sub-arrays. In any event, there is no evidence in the literature of any sea-truthing experiments which could verify this method.

1.5 Scope of Thesis

The purpose of this thesis is twofold. The first objective is to validate the ability of the Cape Race radar to monitor the radial current field. This system is the first of its kind in North America and it was not subjected to any previous validation experiments in this area. Hence, the need for an investigation of this kind is imperative to test and further promote the technique. The second objective is to examine the possibility of using the radial data to estimate total current vectors. This has not been previously attempted using a long-range system. Therefore, an experiment of this nature provides a valuable dataset for testing algorithmns to promote this capability.

In the vector current method presented in this thesis, the radial components are formulated as a system of linear equations which were derived directly from the system geometry. The unknowns in this system are the current components which can be determined from a closed-form solution using a simple regression analysis. This alleviates the errors introduced in linearizing the system of equations derived by the method presented in Lipa and Barrick [17]. The end result is a much simpler procedure which can be easily implemented as a real-time software module in a practical radar system.

The general techniques used to process the radar data are described in Chapter 2. The classical technique used to spectrally analyze the radar data will be summarized, with a description of the current estimation method used to yield the radial currents. This will be followed by the formulation of the vector current algorithmn and its solution.

The experiment is discussed in Chapter 3. Normally, this would be dealt with as an appendix. However, since this is essentially an experimental thesis where the data for model validation was provided by the Northern Radar Cape Race facility from October 20 to November 21, 1992, it is felt that a description of the same is deserving

of a chapter. This also provides an appropriate intermission from the radar theory, as it discusses the experiment from a practical standpoint before the data analysis procedures are presented in the following chapter.

Chapter 4 presents the data analysis procedures used for the drifter and radar data and discusses the possible errors associated with both techniques. The data simulations, which were designed to alleviate the complexities associated with typical radar simulations, are also discussed here.

The results from the data analysis procedures are discussed in Chapter 5. These results provide a comparison of the simulated and the actual radar/drifter current estimates.

Conclusions from this study will be presented in Chapter 6. Finally, some ideas for future developments in this area are considered.

Chapter 2

Technique

2.1 Introduction

The radar coverage zone can be partitioned into a polar grid of radar scattering cells, each of which is specified by the radar's range and azimuthal resolution. A HF Doppler spectrum from each of these cells is characterized by two dominant peaks spaced symmetrically about the carrier. The frequencies of these peaks are used by all HF GWR systems for the measurement of ocean surface currents since they indirectly trace the underlying average surface current component. These components, or radial current projections, can be estimated for all cells in the radar coverage zone to yield a grid of the radial current field. How these data grids are generated will be discussed in the following sections.

For the estimation of vector currents, a technique will be presented which assumes that the current is uniform about the estimation point. In this case adjacent azimuthal radial current components will be different projections of this current. A geometric linear equation describes this relationship for one radar cell. A set of these equations can be generated for all cells which fall within the assumed uniform current region. These equations can then be subjected to a linear regression analysis to yield an estimate of the vector current components.

2.2 Radial Surface Currents

2.2.1 Theory

The motion of the ocean waves is seen by the radar as a translation of the frequency of the received echo signal from that of the carrier. In keeping with the Bragg scattering phenomenon, the dominant received radiation is resonant scattering from ocean waves travelling towards or away from the radar and having a wavelength one half that of the transmitted signal. In this mode, the radar emulates an ocean wave spectrometer since it predominantly observes only these wavetrains. This interaction induces on the radar Doppler frequency spectrum symmetrically spaced peaks whose positions are dictated by the phase velocities of the advancing and receding wavetrains, respectively. In the HF community, these are commonly referred to as Bragg lines. In the absence of currents, these lines have well defined Doppler frequencies. If a current exists beneath the surface waves, the radar sees this as a translation of the co-ordinate frame of the scattering wave trains. This imparts another frequency shift on the Bragg lines which is proportional to the radial component of the current velocity along the radar receiving direction[1].

The following short mathematical explanation of the above process will be presented next since it concisely summarizes the above paragraphs. For an excellent introduction on fundamental radar principles the reader should refer to the text "Radar Principles" by Nadav Levanon[43].

It is well established that for grazing incidence, the velocity, V_b, of the Bragg wave as derived from the deep water gravity wave dispersion relation is given by

$$V_b = \pm\frac{1}{2}\sqrt{\frac{g\lambda}{\pi}} \tag{2.1}$$

[1]The details of the mathematical derivations of the above concepts and the scattering mechanisms will not be presented here since these are based on fundamental radar principles. Instead, only the principal equations governing Doppler shifts which originate from moving targets will be considered.

where λ is the radar wavelength and g is the acceleration due to gravity. The corresponding Bragg frequency, f_b, induced on the Doppler spectrum due to the motion of the wavetrain in the absense of surface currents is given by

$$f_b = \sqrt{g/\pi\lambda} \tag{2.2}$$

which at 6.75 MHz is 0.2651 Hz. The existence of surface currents shifts the dominant peaks from their theoretical values as in shown by the example presented in Figure 2.1. The difference between the frequency of the theoretical Bragg wave and the one determined from the radar data is a measure of the average radial component of the surface current to a depth of approximately $\lambda/8\pi$ m (Stewart and Joy [8]). This is approximately 2 m for a radar operating at 6.75 Mhz.

Since the radial current measurement consists of determining the shift Δf from its theoretival value of f_b, from the above equations it can be shown that the radial component v_r of the surface current within a radar scattering cell is

$$v_r = 0.5\Delta f\lambda \tag{2.3}$$

for an ideal HF radar system.

2.2.2 Measurement

To remotely measure ocean surface currents from a HF system, the azimuthal resolution provided by the receiving antenna beam and the radar's range resolution are used to isolate the radar return from a resolution cell on the ocean surface. The radar echo fluctuation from this cell is indirectly sampled at the waveform repetition frequency and the resulting time series of samples are subjected to a Fast Fourier Transform (FFT). This generates the Doppler frequency spectrum.

From Section 2.2.1, it is clear that the accuracy of the current measurement is dependent on the accuracy of the computation of the frequency of the two Bragg

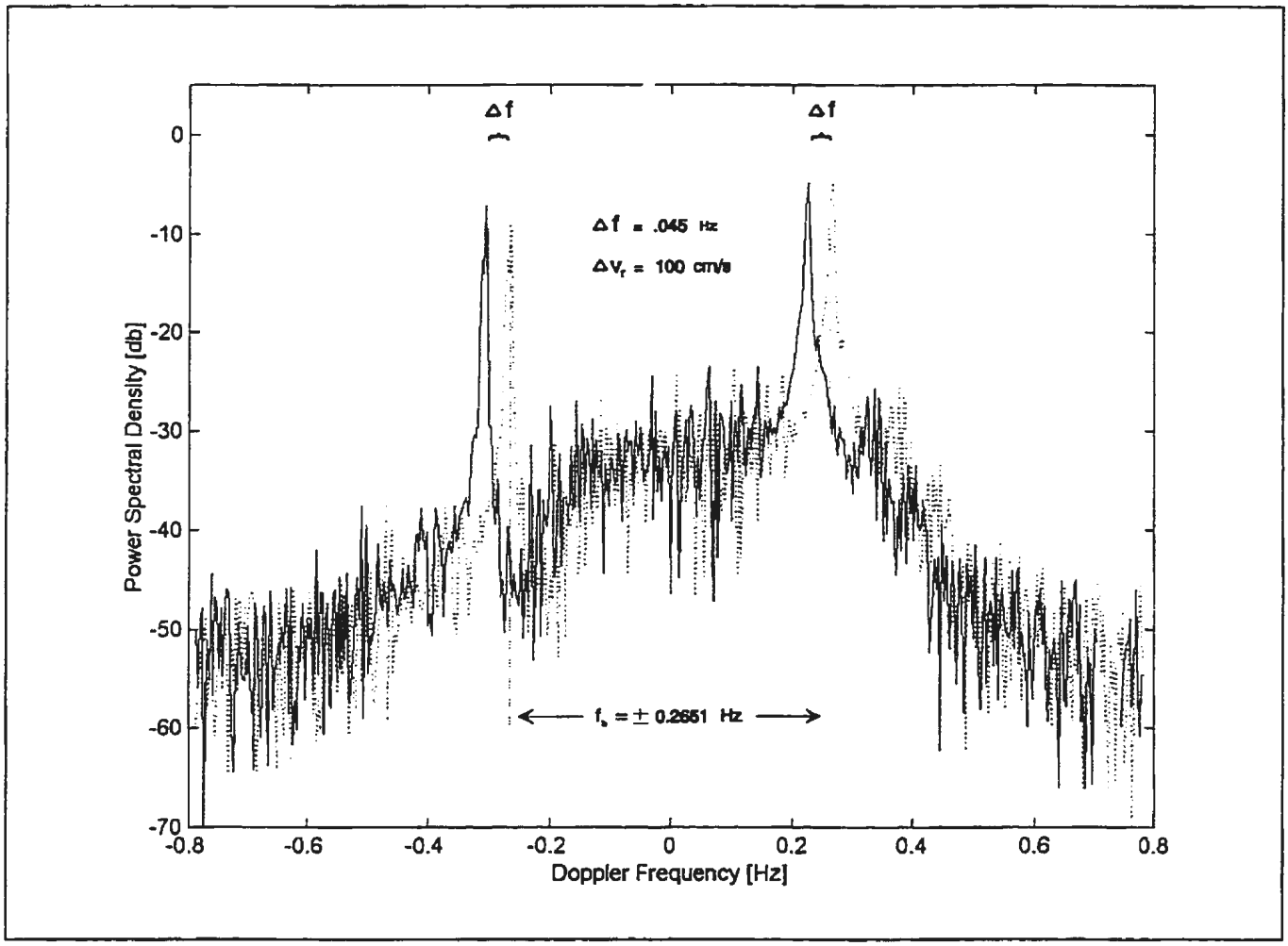

Figure 2.1: Radar Spectrum (solid line) from 6.75 MHz operation. An underlying current with a radial component of approximately 100 cm/s and moving away from the radar induces a Doppler shift of approximately 0.045 Hz on the spectrum observed with no underlying current (dashed line).

peaks. Since the frequency computation is performed by using a standard software FFT implementation, the frequency resolution of the spectrum is the reciprocal of the time interval, in seconds, over which the data from each cell is sampled. This time interval or coherent integration time (CIT) restricts the radar's ability to "pinpoint" the true Doppler frequency using the periodogram approach[2]. Hence,the actual peak may be 'somewhere between' two adjacent frequency bins. The estimation of the 'mean', or centre frequency, of a spectral peak is performed with the commonly used

[2]It is also assumed that radial current deviations caused by beam direction errors are insignificant as compared to the current resolution provided by the FFT.

'centroid' definition, while an estimate of the error in this calculation is provided by the FFT resolution. Thus, a radial current estimate, as well as an estimate of its error, is obtained from each radar spectrum.

To illustrate the above concepts, an example is presented using the system parameters of the Cape Race radar, namely those associated with the radar's spatial and Doppler resolutions. The azimuthal resolution of a linear array is approximately λ/D radians where λ is the radar wavelength and D is the length of the array (Collin [44]). Since the receive array at Cape Race, circa 1992, was 866 m in length and the centre radar frequency was 6.75 Mhz, the approximate radar beamwidth is 3 degrees[3]. The radar's range resolution is determined by the bandwidth, f, of the transmit waveform and is given by $c/(2f)$ where c is the velocity of light. Since the radar transmission bandwidth used to generate the experimental data of this report was 375 kHz the range resolution for the experiment is approximately 400 m. Therefore, the cell size at ranges of 50, 100 and 200 km are approximately 1, 2 and 4 square km, respectively. To determine the approximate current frequency resolution we need to refer to the waveform repetition interval which, for the experimental data, was approximately 0.6 seconds. Typically 512 samples were collected at this sampling interval, per radar beam, to yield a CIT of approximately 300 seconds. Since the frequency resolution is the reciprocal of this time interval, the resultant Doppler resolution is approximately .003 Hertz. The corresponding current velocity resolution, using Equation 2.3, is approximately 7 cm/s. In other words, the current estimate is approximate to within ± 3.5 cm/s of the FFT estimate. The azimuth associated with this estimate is obtained by the appropriate phasing of the received signal at each antenna. Therefore, to cover a selected azimuthal extent in the radar coverage zone, we can dwell in a direction for a time interval, Δt, then 'shift direction and dwell' until the region is covered. We can therefore generate radial velocity estimates at range and angular

[3]This assumes that each element is an isotropic sensor. However, the beamwidth actually varies from approximately 2.5° to 6.0° because of the sub-array patterns.

intervals of Δr and $\Delta\theta$, where these parameters are the nominal radar range resolution and beamwidth, respectively. (See Khan *et al.* [45] for a complete description of the design of the Cape Race system).

2.3 Vector Surface Currents

2.3.1 General Problem Formulation

A region, S, of range resolution Δr and azimuth resolution $\Delta\theta$ in the coverage area of a HF radar is considered. It is assumed that a uniform surface current, $\vec{V}$, exists in S during the dwell time for this region. This geometry is shown in Figure 2.2 where the radar is situated at the origin.

Let the unit vector $\hat{e}_j$ point in the direction of the centre of a radar receive beam such that it makes an angle Θ_j with respect to the x-axis of the co-ordinate system. Let the uniform current vector, which projects itself along the beam direction, be denoted by $\vec{\mathbf{V}}$. Hence, at the position (r, Θ_j) in S, a radial current measurement will be monitored by the radar.

In this co-ordinate system, $\vec{V}$ is

$$\vec{V} = V_x\hat{x} + V_y\hat{y} \tag{2.4}$$

where $\hat{x}$ and $\hat{y}$ are unit vectors along the x- and y- axis, respectively and V_x and V_y are the components of $\vec{V}$. Since we can represent the unit vector in the radial direction perpendicular to $\hat{\Theta}_j$ as

$$\hat{e}_j = \cos(\Theta_j)\hat{x} + \sin(\Theta_j)\hat{y} \tag{2.5}$$

and the radial component of $\vec{V}$ along this direction as

$$v_j = \vec{V} \cdot \hat{e}_j \ , \tag{2.6}$$

it follows that

$$v_j = V_x \cos(\Theta_j) + V_y \sin(\Theta_j) \tag{2.7}$$

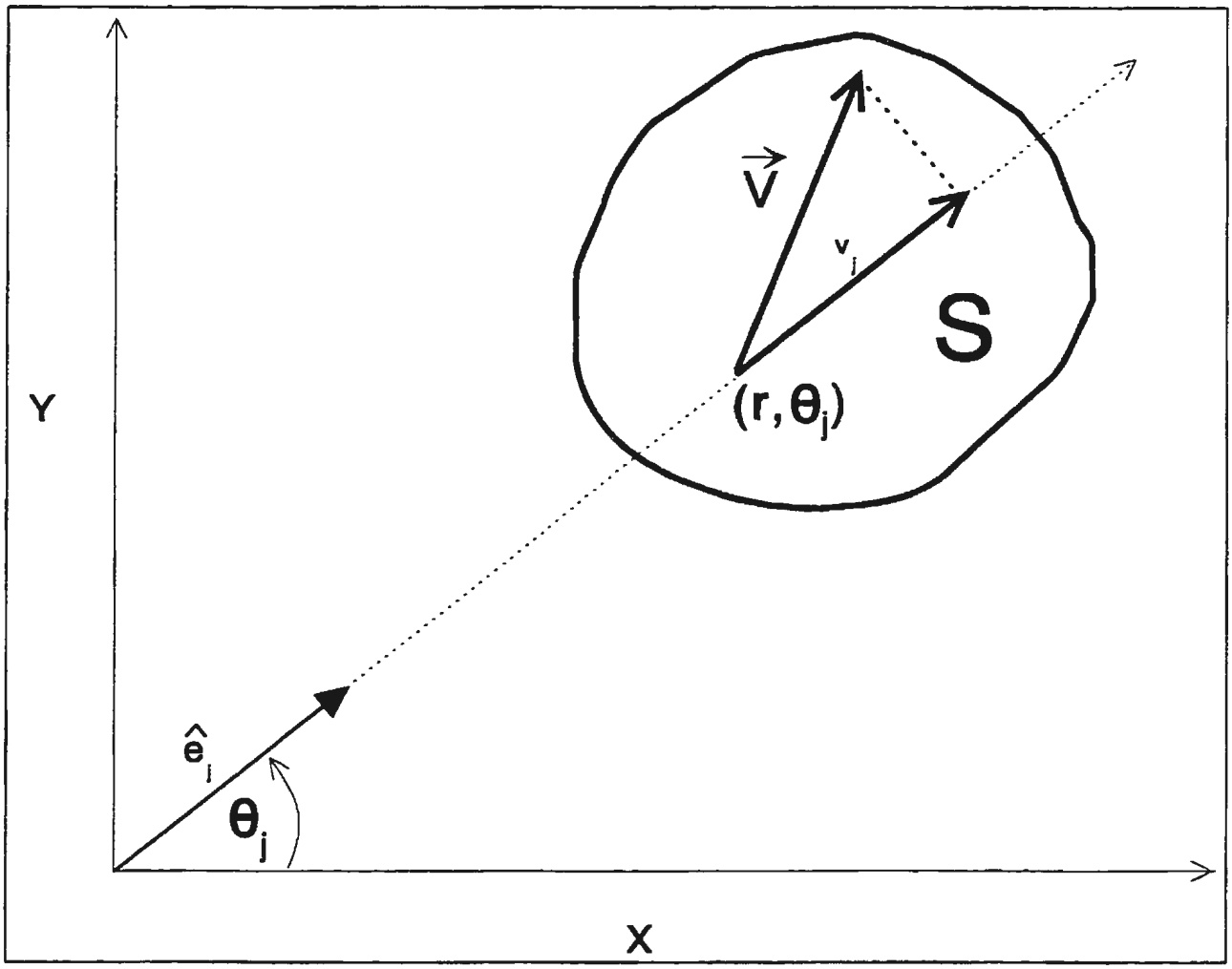

Figure 2.2: Geometry of region S where a radial current component is being measured along the direction $\hat{e}_j$

which is the projection of $\vec{V}$ along the direction of $\hat{e}_j$.

Next, a subset of region **S**, say **Q**, is considered. The total radial and angular extents of **Q** are ΔR and $\Delta\Theta$, espectively. Further, the region **Q** is subdivided into sub-sectors of range extent Δr and angular extent $\Delta\theta$ such that

$$\Delta R = m \times \Delta r \tag{2.8}$$

and

$$\Delta\Theta = \sum_{i=0}^{n-1} \Delta\theta_i \ , \tag{2.9}$$

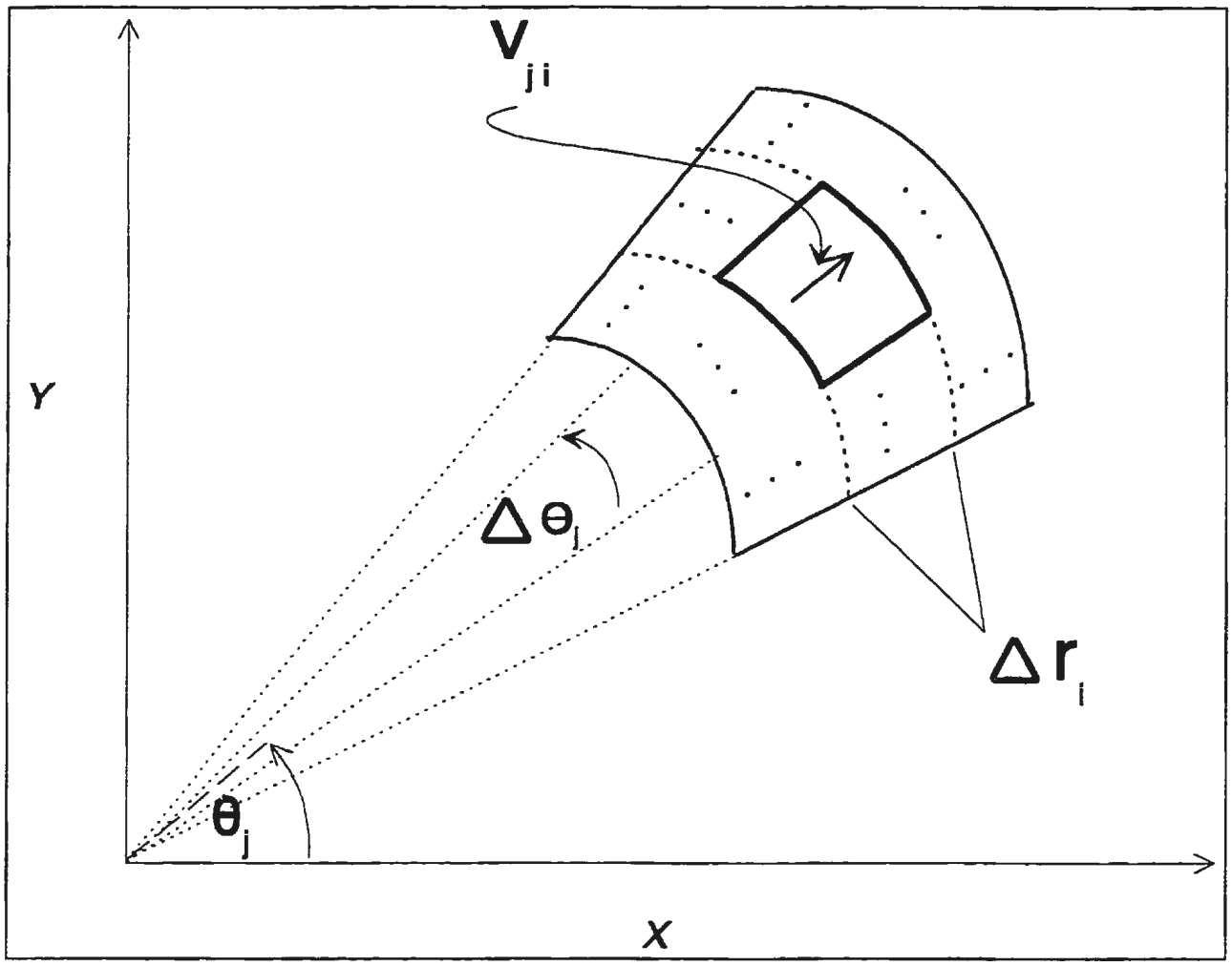

Figure 2.3: Region Q is subdivided into $m \times n$ sub-regions, where each sub-region, ij, is monitored by the radar to give a radial component v_{ij} along the $\hat{e}_j^{th}$ direction and the i^{th} equi-distant cell from the radar.

where n beams intersect the region and $\Delta\theta_i$ is the beamwidth of beam number i. This geometry is shown in Figure 2.3.

Let the m range cells within Q be indexed from 0 to $m-1$ and let a range cell within this range be indexed by i. Let's consider the radial current from the ij^{th} cell, where j is the index of the beam which makes an angle Θ_j with the x-axis. Since this current obtained from an actual radar system consists of an error component, ϵ_{ij}, equation (2.7) may be rewritten as

$$v_{ij} = V_x \cos(\Delta\Theta_j) + V_y \sin(\Delta\Theta_j) + \epsilon_{ij} \tag{2.10}$$

Let Θ_0 be the smallest angle a beam in $\mathbf{Q}$ makes with the x-axis. Therefore, if n beams intersect this region we have for n radial projections, $v_0, v_1, \cdots, v_{n-1}$ of $\vec{V}$ in the i^{th} range sector of $\mathbf{Q}$

$$\begin{aligned}
v_{i0} &= V_x \cos(\Theta_0) + V_y \sin(\Theta_0) + \epsilon_{i0} \\
v_{i1} &= V_x \cos(\Theta_1) + V_y \sin(\Theta_1) + \epsilon_{i1} \\
\vdots &\quad \vdots \qquad\qquad \vdots \\
v_{i(n-1)} &= V_x \cos(\Theta_{n-1}) + V_y \sin(\Theta_{n-1}) + \epsilon_{i(n-1)}
\end{aligned}$$

Over the entire region, $\mathbf{Q}$, there are m sets of such equations which may be cast as

$$\begin{aligned}
v_{00} &= V_x \cos(\Theta_0) + V_y \sin(\Theta_0) + \epsilon_{00} \\
\vdots &\quad \vdots \qquad\qquad \vdots \\
v_{0(n-1)} &= V_x \cos(\Theta_{n-1}) + V_y \sin(\Theta_{n-1}) + \epsilon_{o(n-1)} \\
v_{10} &= V_x \cos(\Theta_0) + V_y \sin(\Theta_0) + \epsilon_{10} \\
\vdots &\quad \vdots \qquad\qquad \vdots \\
v_{1(n-1)} &= V_x \cos(\Theta_{n-1}) + V_y \sin(\Theta_{n-1}) + \epsilon_{1(n-1)} \\
\vdots &\quad \vdots \qquad\qquad \vdots \\
v_{i0} &= V_x \cos(\Theta_0) + V_y \sin(\Theta_0) + \epsilon_{i0} \\
\vdots &\quad \vdots \qquad\qquad \vdots \\
v_{ij} &= V_x \cos(\Theta_0) + V_y \sin(\Theta_0) + \epsilon_{ij} \\
\vdots &\quad \vdots \qquad\qquad \vdots
\end{aligned}$$

$$
\begin{aligned}
v_{i(n-1)} &= V_x \cos(\Theta_{n-1}) + V_y \sin(\Theta_{n-1}) + \epsilon_{i(n-1)} \\
\vdots \quad & \quad \vdots \qquad\qquad \vdots \\
\vdots \quad & \quad \vdots \qquad\qquad \vdots \\
v_{m0} &= V_x \cos(\Theta_0) + V_y \sin(\Theta_0) + \epsilon_{m0} \\
\vdots \quad & \quad \vdots \qquad\qquad \vdots \\
v_{m(n-1)} &= V_x \cos(\Theta_{n-1}) + V_y \sin(\Theta_{n-1}) + \epsilon_{m(n-1)}
\end{aligned}
$$

The above system of equations is severely over-determined since we have 2 unknowns in $m \times n$ equations. However, the solution of such a system is well known and will be discussed in the following section.

2.3.2 Solution

Consider the system of equations which were derived from the previous section. If we let the radial current components be written as

$$
\vec{v} = \begin{pmatrix} v_{10} \\ v_{11} \\ \vdots \\ v_{m(n-1)} \end{pmatrix}
$$

and the error terms as

$$
\vec{\epsilon} = \begin{pmatrix} \epsilon_{10} \\ \epsilon_{11} \\ \vdots \\ \epsilon_{m(n-1)} \end{pmatrix}
$$

This allows us to write

$$
\vec{v} = \vec{\Phi}_1 V_x + \vec{\Phi}_2 V_y + \vec{\epsilon} \tag{2.11}
$$

where

$$
\vec{\Phi}_1 = \begin{pmatrix} \cos(\Delta\Theta_0) \\ \cos(\Delta\Theta_1) \\ \vdots \\ \cos(\Delta\Theta_{n-1}) \end{pmatrix}, \vec{\Phi}_2 = \begin{pmatrix} \sin(\Delta\Theta_0) \\ \sin(\Delta\Theta_1) \\ \vdots \\ \sin(\Delta\Theta_{n-1}) \end{pmatrix}
$$

This is an example of a multiple regression model with two regressors. The model is non-linear in the two regressor variables, Φ_1 and Φ_2, but it is linear in the unknown regression coefficients V_x and V_y. If we assume the error terms, ϵ_i, in the model have zero mean and constant variance, and that the errors are uncorrelated, we can proceed to use standard regression techniques to estimate the surface current parameters V_x and V_y.

Chapter 3

Experimental Data

3.1 Introduction

The prime objective of this research is to investigate the surface current sensing capabilities of a long-range, single-station, HF GWR. This has been documented with two-station, short-range HF installations, as described in the literature review of Chapter 1. However, it has not been documented using a single long-range system. A single long-range station, for example, with a range and azimuthal coverage of approximately 250 km and 120°, has the potential to map an area of approximately 66,000 square kilometers. Therefore, agencies responsible for monitoring the exclusive economic zones of coastal nations may find data products from such a system to be extremely informative, timely, and cost-effective. As a result of shrinking national budgets for such services, joint ventures involving many nations have evolved. For example, the experiment upon which this thesis is based was part of a larger study by the Canadian and U.S. Coast Guards, as well as the Canadian Department of Fisheries and Oceans (DFO). Their primary goal is to improve the drift predictions of search and rescue models. Presently the search and rescue models lack adequate surface current data for the estimation of search regions. Therefore, the information provided by a HF system could enhance the usefulness of these models.

Another objective of HF radar experiments is for fisheries research since currents play a role in nutrient transport. The DFO was interested in the ability of HF GWR to

estimate ocean surface currents since the late 1980's when a portable HF system was deployed to map currents in Conception Bay, NF. This system, the CODAR which was introduced in Chapter 1, consists of two stations which measure the components of the surface current field radial from each station to a range of approximately 30 km in polar increments of 1.2 km and 5°. In this way, the vector current field may be calculated from strictly geometric considerations by using the radial current grids produced from each station (Barrick *et al.*[46]). Since surface currents play a major role in the dispersion or 'flushing out' of fish larvae contained in these inlets, this system could provide a clearer picture, both temporally and spatially, of the current circulation patterns which DFO had difficulty in obtaining via *in situ* methods. DFO was only capable of monitoring Eulerian currents and a few Lagrangian measurements with drifters. This was a very time consuming exercise that provided sparse current vectors as compared to the radar technique, which could provide a map of the circulation patterns on an hourly basis. Since many of the standard instruments, such as current meters, must be deployed to obtain the measurement scale that DFO required, the CODAR system was ideally suited for their data requirements. For example, a grid of current data could be constructed with a resolution of approximately 1.2 km over a 2000 square km zone.

The DFO was also interested in the current patterns over the Grand Banks since these currents affect nutrient circulation in this rich fishing zone. Since the portable system did not have the capability for these long range measurements, an alternative system was needed. This new system was built in 1990 at Cape Race, by NRSL, from local government and investor funding. It was designed primarily as a ship detection radar system but it was also capable of mapping currents. The radar has been demonstrated to have a nominal range of 200 km over a 120° sector, which entailed a large portion of the the Grand Banks. Even though this system could measure only the radial components of the current field it was envisioned that other systems would

be built at other coastal sites such that the vector field may be constructed between stations with dual coverage. Hence, it was advantageous for DFO to become involved at this stage of the program development since the data products provided by these modern radar systems could aid in future fisheries research, especially in light of the collapse of the cod fishery in Newfoundland.

3.2 The Drifter Component

The experiment commenced on October 20, 1992 with the deployment of three Seimac Limited of Canada Accurate Surface Tracker (AST) buoys on the Southern Grand Banks (Figure 3.1).

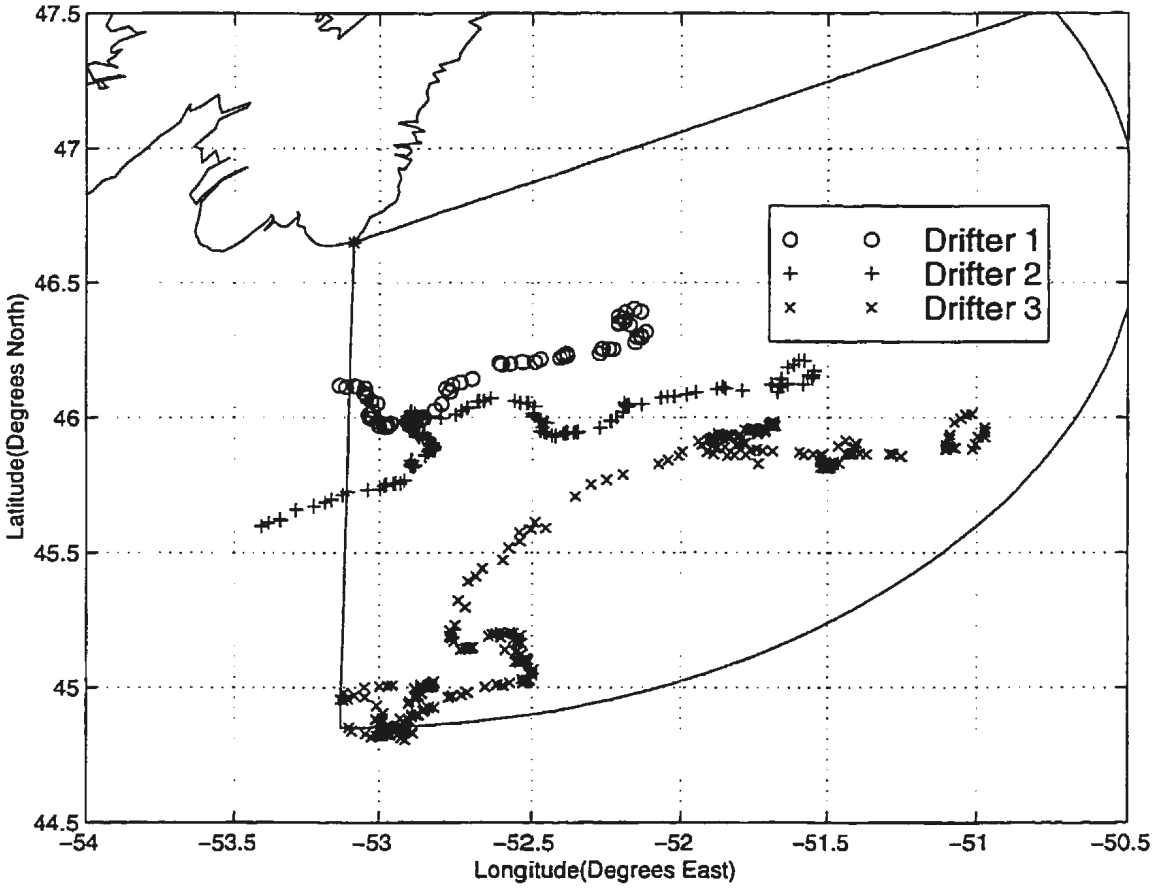

Figure 3.1: The positions of the three Accurate Surface Tracker drifters as recorded by the satellite system. This raw positional data was subsequently used to estimate the drifter velocities.

Drifter positions were obtained from the ARGOS satellite system, in near real time, approximately 10 times daily. The 0.5-m diameter by 1.0-m long barrel-shaped AST buoys were designed to accurately track the drift of the top metre of the ocean. Although these buoys are not drogued, they are designed to fill with water on deployment and are bottom weighted so that they remain upright. Extensive trials during the Canadian Atlantic Storms Project, as documented by Anderson and Shaw [47], proved that they have excellent drift characteristics. At 6.75 MHz the radar provides an average current velocity for about the top 2 m of the water column (Stewart and Joy [8]). Thus, the buoys and the radar sampled essentially the same oceanographic regime.

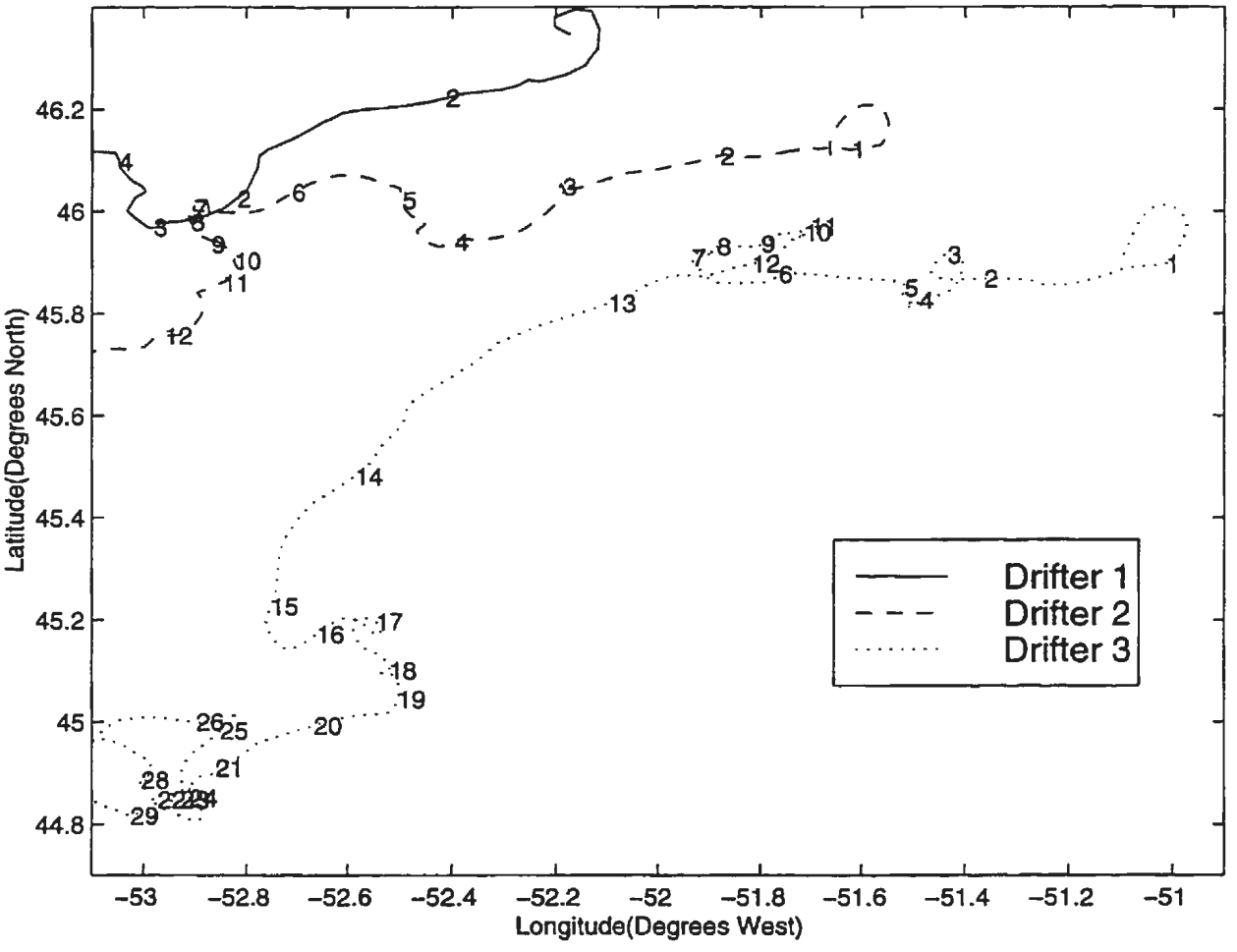

Figure 3.2: An enhanced view of the three AST drifter tracks with the numbers indicating days of the experiment on which the radar collected surface current data.

Since the mean currents within most of the radar coverage zone are weak (□ 20 cm/s, Petrie and Anderson [48]), and since the surface flow in the autumn storm season is generally dominated by directly wind-driven currents, the buoys were deployed in the centre of the coverage zone along the broadside look direction of the radar (120°T), at ranges of 75, 125 and 175 km. Unfortunately, a tropical storm stalled over the Grand Banks shortly after deployment and its steady northeasterly winds quickly drove the inner two buoys towards the edge of the radar coverage. Buoy 1, deployed at a range of 75 km, stayed within view fewer than 5 days and returned only 6 radial velocity intercomparisons; Buoy 2, deployed at 125 km, survived for 12 days and provided 23 comparisons; fortunately Buoy 3, deployed at 175 km, remained within range for most of the experiment and yielded 48 useful comparisons.

3.3 The Radar Component

3.3.1 Radar System

The radar system, designed, owned and operated by NRSL, is located on a 2.5 km strip of land along the coast at Cape Race, as shown in Figure 3.3.

The HF GWR site consists of receive and transmit antennas, a receive/control and accomodations building, and a transmit building. The transmit antenna is a log-periodic dipole array antenna with a half-power beamwidth of 120°(over perfect ground), a peak power rating of 10 KW, and an average power of approximately 1 KW. The transmitted waveform is a frequency modulated interrupted continous wave (FMICW) where the carrier is swept over 375 kHz to obtain a range resolution of approximately 400 m. An operating frequency range between 5 and 8 MHz was available, but the two frequencies used in this experiment were 6.25 and 6.95 MHz.

A block diagram of the system architecture is shown in Figure 3.4. The 40-element phased array is partitioned into ten 4-element sub-arrays which can be electronically phased, via analog beamforming units, to form a sub-array pattern. Instead of the

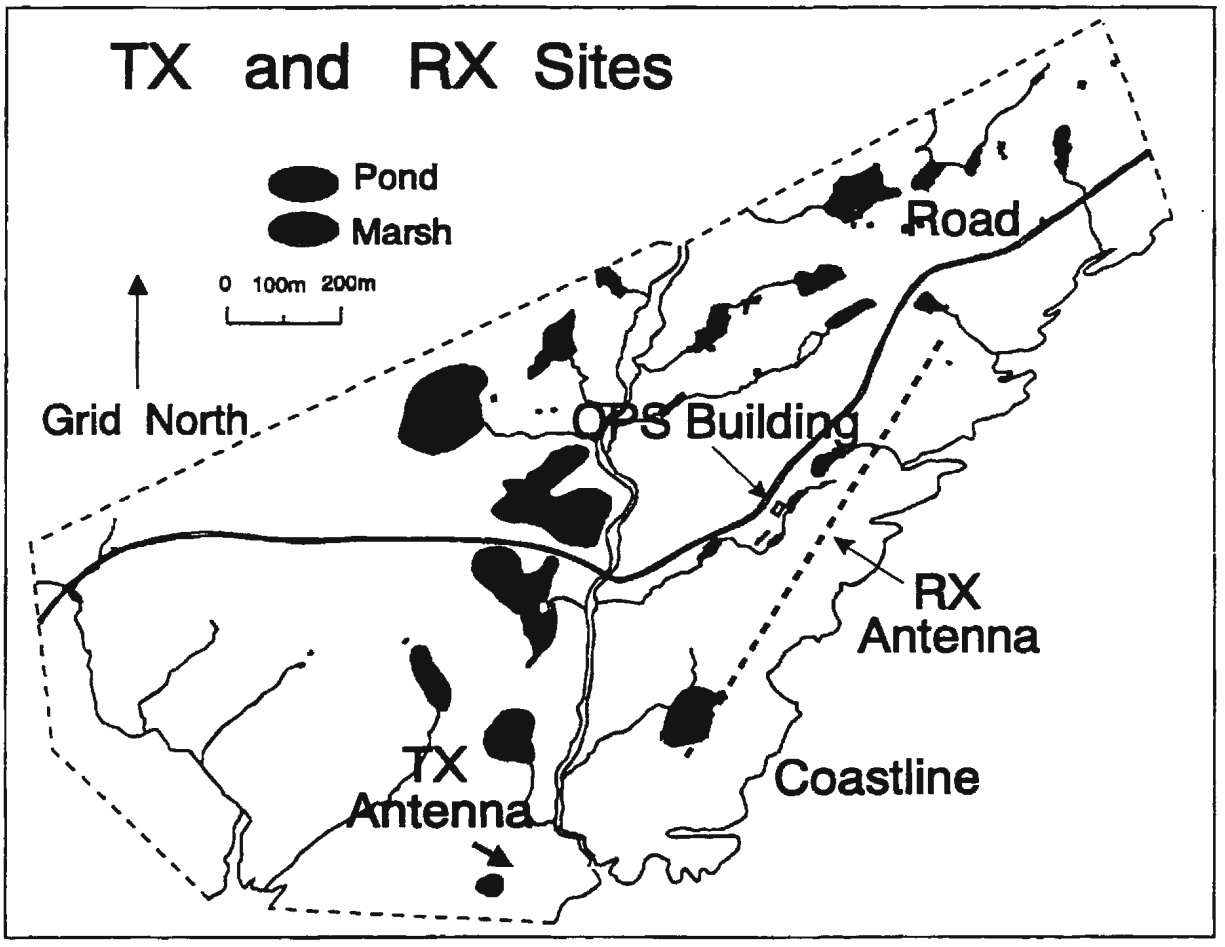

Figure 3.3: Layout of Cape Race radar site

approximate $\lambda/4$ element spacing of the original array, the effective antenna element separation of the 10 channel sub-array system is now approximately 2λ. Subsequent beamforming in software of these 10 channels can steer the resultant main lobe to any direction within the sub-array pattern. Subsequently only ten receivers, as opposed to 40, are required to perform the waveform demodulation and analog-to-digital conversion. The pre-processor unit performs the range discrimination, via the FFT, on a pulse-per-pulse basis using 12 inter-leaved digital signal processing units. Doppler processing is performed on a VAX 11/785 system for subsequent analysis and display.

The receiving antenna is an 866 metre phased array consisting of 40 planar diamond-shaped monopoles. The beamwidth increases from approximately 3.0° broadside to 6°, with 60° steering from broadside. The total angular coverage, which in-

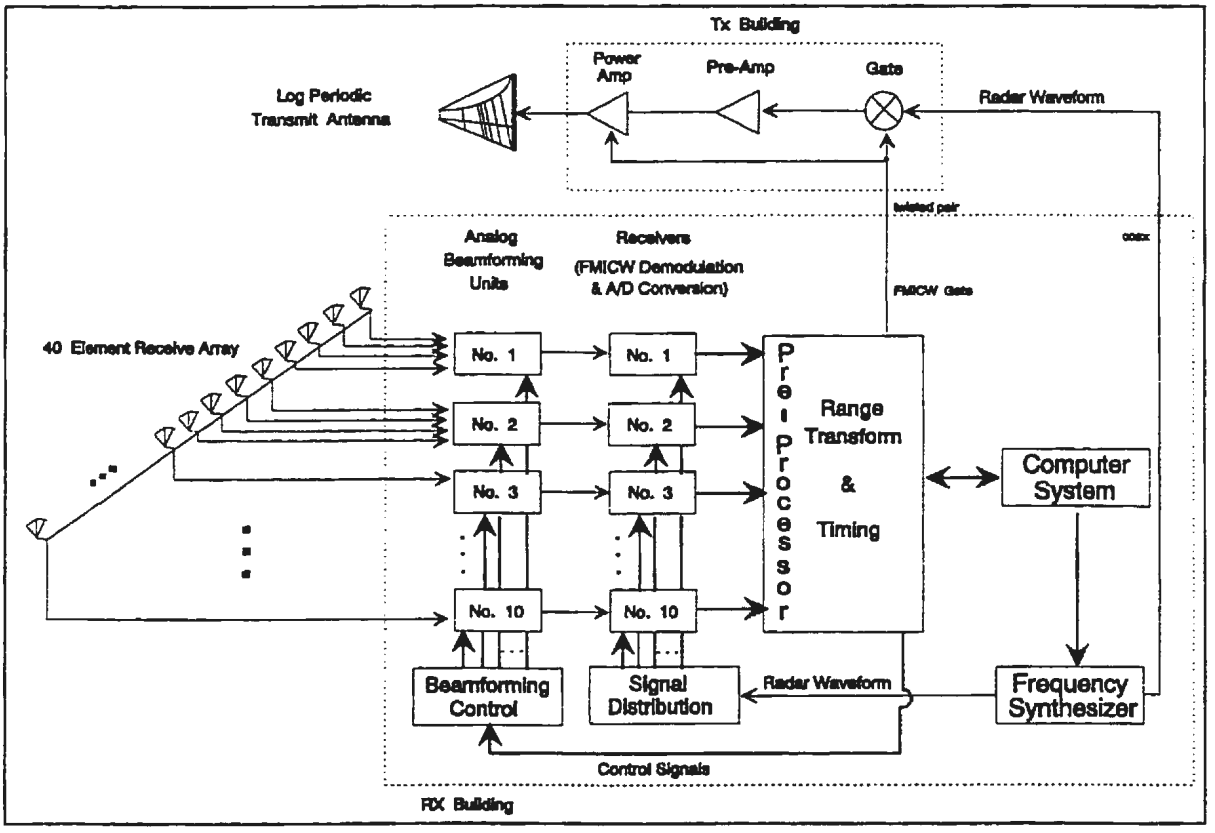

Figure 3.4: System architecture of Cape Race radar

cludes a large portion of the Grand Banks as shown in Figure 3.5, is from a bearing of 61° to 181° (True). The interested reader is referred to Khan *et al.* [45] for a more complete description of the radar system.

3.3.2 Operations

The radar began tracking the buoys on October 21, 1992, and was turned off on November 22, 1992. Typically, one to three radar measurements were made daily between the hours of 09:00 and 17:00 local time (Figure 3.2). However, data were rendered unuseable on day 2 (Julian day 296) due to data collection software errors and on days 22–25 (Julian days 316 – 319) when hardware beam forming problems were encountered. (See Appendix A for a chronology of the experiment).

Since the surface currents of the Grand Banks region are normally less than 50 cm/s, the positions of the drifters were not expected to vary appreciably in a daily

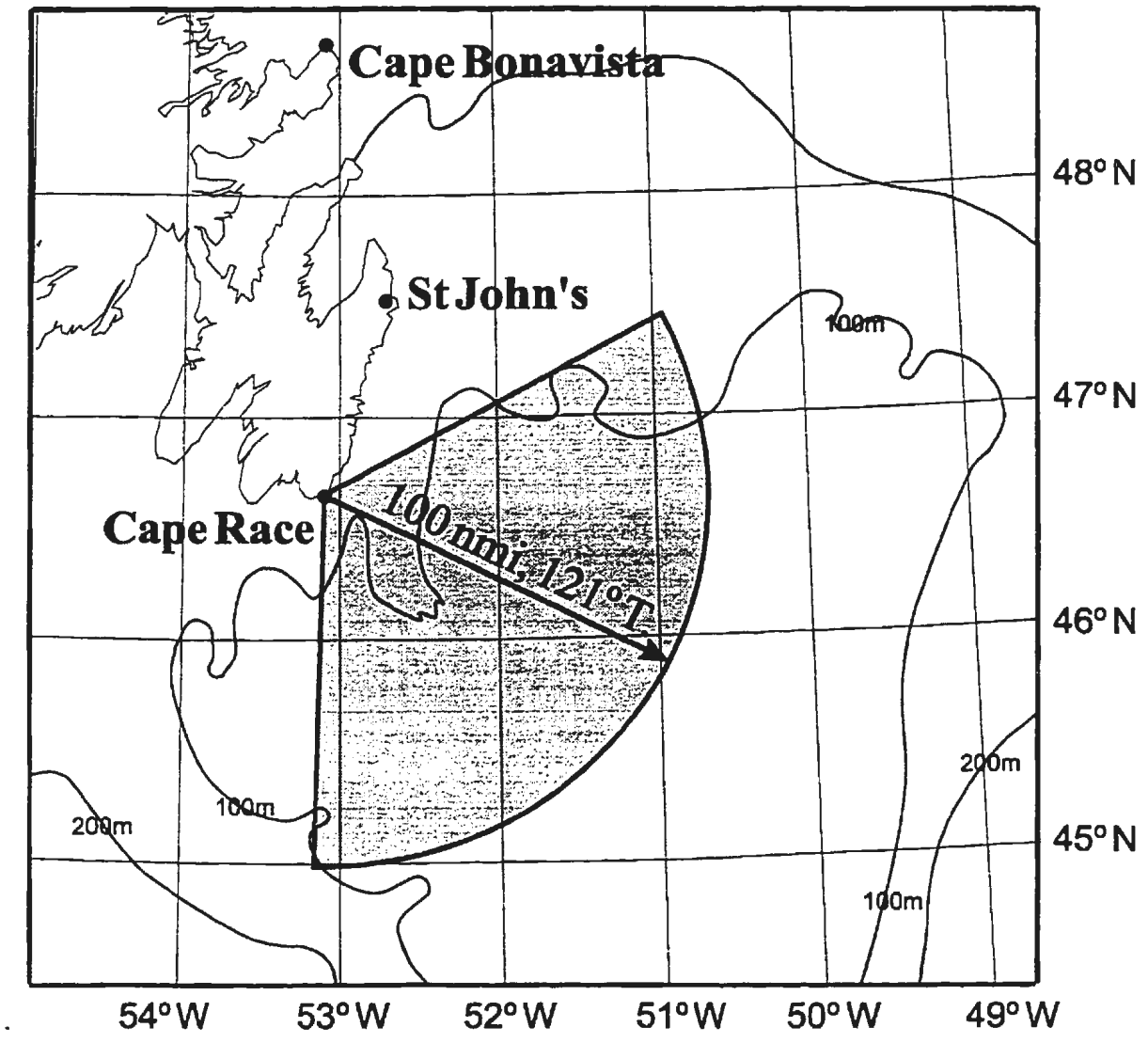

Figure 3.5: Coverage Region off Cape Race

period. As a result of this, and to reduce the data volume, the radar usually only scanned a region in the vicinity of the drifter positions. For example, the first recorded positions each day were relayed to the radar operator from DFO and were used to select a mimimum 60-km-in-range by 60°-in-azimuth sectors centred on each buoy. Within the sectors the radar achieved an approximate 400-m by 4° resolution, which translates to 400 m by 5.2 km at 75 km range, or 400 m by 12.2 km at 175 km range. In addition, larger datasets consisting of current measurements of the total radar coverage area were surveyed daily to measure the larger-scale surface current

spatial variability and to check system performance. These sector extents are noted in Appendix C.

As a data quality check the radar was continually monitored on a per data run basis. Plots of the returned radar signal were regularly produced to inspect range performance. On-line spectral processing was also performed to determine the quality of the Bragg components. Also, as they became available, most radial surface current maps were inspected for obvious errors.

Field personnel were stationed at the radar site for the duration of the experiment so that hardware problems could be quickly addressed.

3.3.3 System Performance

There was one hardware failure noted during the experimental period. An inspection of the system on the morning of the 15^{th} of November (Julian day 320) revealed that 2 of the 10 beamforming units were defective. The defective units were immediately replaced. It was later determined these units were causing problems on November 11^{th} (Julian day 316), as revealed by a degradation in the data quality from that day to the day of unit replacement. Other data losses, though very mimimal, were mainly due to minor software problems that occurred during the initial stages of the program. (See Appendix A, for the experimental chronology).

The maximum radar range was observed to be approximately 300 kilometers, with a minimum range of approximately 200 km. This was sufficient for an experiment of this nature since the drifter positions never exceeded 200 km.

Chapter 4

Data Analysis

4.1 Introduction

The drifter and radar data analysis procedures are briefly described in this chapter. The drifter analysis procedure will describe how the current velocites are derived from the positional data recorded by DFO from the ARGOS satellite system. However, since this technique has been reported elsewhere (Helbig [49]), it will only be briefly discussed. Similarly, for the radar description, only the high-level processing techniques will be presented since the fundamental details of the radar system design, and its implementation, have been previously reported (Khan *et al.* [45]).

A discussion of the radar data processing methods will be partitioned into two sections. The first section deals with the processing of the radar time series data after it has been beamformed into a grid of range-azimuth bins. The radial current algorithmn processes the time series and generates a polar grid of radial current speeds from the resultant spectra. This is the fundamental analysis step since this data, when compared to similar data from another sensor, illustrates the radar's ability to sense the radial component of the current. The second section deals with the vector current processing data analysis. This analysis entail, the selection of the primary algorithmn parameters, some processing considerations, data reduction of the polar grid to match the algorithmn parameters, and the final processing step which yields the orthogonal current components. The current estimates provided by

both of these techniques can then be compared to the results from the drifter analysis. Both simulated and actual data will be subjected to the algorithmn.

4.2 Drifter Data

Weighted splines were fitted to the northerly and easterly co-ordinates of each drifter track to form an evenly spaced time series, with three hour intervals, of position and velocity as described by Helbig [49]. Weights were chosen to be inversely proportional to the estimated quality of each positional fix, as supplied by Service Argos. The data were not low-pass filtered and extensive simulations by Helbig [49] indicated the resultant speeds exhibited standard deviations of about 5–7 cm/s.

The gist of the drifter velocity calculation is to differentiate the splined-fitted positional data. It should be noted that although the spline fitting and differentiating is intended to smooth irregularities from the drifter tracks, the derived velocities are not equivalent to the radar results since they contain information at scales which may be different than those measured by the radar. The drifter estimate is Lagrangian in nature, giving an average value over a portion of a track. However, the radar measure is Eulerian, being an average estimate over the radar resolution cell, which may be several square kilometers. Therefore, the drifter and radar estimates may never truly equate unless the current is uniform over a region that is large, with respect to the dimensions associated with both estimates. However, this is the only known reliable technique to test the radar current estimates since currents near the surface are extremely difficult to monitor.

4.3 Radar Data

Data from each radar beam direction was sampled at a rate of approximately 1.7 Hz, as described in Section 2.2.2. This unambigously displays the spectral content of the signal to approximately ± 0.8 Hz, which is sufficient for current measurement

since at 6.75 MHz the Bragg frequencies are approximately ± 0.25 Hz. The nominal dwell time, or time to collect a series of consecutive echo pulses, was approximately 300 seconds. Therefore, approximately 512 samples were obtained and spectrally processed to give an FFT bin resolution of approximately 0.0033 Hz. This yielded a current velocity resolution of approximately 7 cm/sec.

During any dwell period, signals at the receivers are combined to yield a constructive signal from one coarse direction only (See Section 3.3.1). The radar was configured to yield 31 coarse beams, each separated by approximately 4°. Therefore, a selected extent in azimuth may be covered by dwelling on a coarse beam for a time interval, say Δt, at one extreme azimuth and then 'shifting' the beam direction and 'dwelling' until the required azimuthal extent is covered. Directions between the coarse beams can be synthesized by fine beam steering, in software, the coarse beam data to generate time samples at range and angular intervals of Δr and $\Delta\theta$, respectively, where Δr is the radar range resolution and $\Delta\theta$ is the nominal radar beamwidth. This fine beam steering calculation is the spatial equivalent of the frequency estimation problem in that the frequency resolution can be improved by either increasing the sampling interval, collecting more samples, or both. In the beamforming case, the number of directions is increased by choosing an appropriate angular increment and introducing new phase factors to fine-steer the coarse beam data. This angular increment is usually some integral factor of the beamwidth (Collin [44]).[1]

Time samples from each range-azimuth cell were spectrally processed using an FFT routine to yield the Doppler information.[2] Since the frequency placements of

[1]Beamforming using a linear array will not be discussed here since it is a standard procedure in radar signal processing. We will note, however, that all sidelobes for the beams synthesized for this study were at least 12 dB below the main beam lobe maximum. See Davis [50] for a description of the beamforming technique used in the radar system at Cape Race.

[2]It is important to mention that Δt should be sufficiently small such that the currents remain constant as we shift from beam to beam, otherwise the assumption of current uniformity will be violated and the vector current algorithmn results may be difficult to interpret. As a note, it has previously been shown that the sea has statistically stationary properties over intervals from 1 to 12 hours (Barrick and Snider [51]). Therefore, since a typical scan of the radar coverage region requires approximately 1 hour, we will assume that the currents are not changing appreciably during this

the dominant, or Bragg, peaks of the spectrum have to be isolated, the data analysis method is one of peak detection. These peak frequency positions were determined from the spectra of each range-azimuth cell using the following steps:

1. A 150 cm/s window was placed about $\pm f_b$ such that the two frequencies with greatest spectral power could be isolated. These two peaks are the signals of interest since they will typically be due to the Bragg waves if there is sufficient wave energy for both components. If the radar frequency is 6.75 MHz then this corresponds to a Doppler frequency window of ± 0.0675 Hz about the Bragg frequency. This window, called the signal window, was chosen to ensure the detection of the largest expected current velocities in the experimental area (Petrie and Anderson [48]);

2. A noise floor was calculated from the average power of all signals in the region 0.5 Hz $< |F| <$ 1.0 Hz where F is the Doppler frequency range. Because there are potentially two Bragg signals per radar spectra, one from the negative and positive halves of the Doppler spectrum, this computation results in two signal and two noise power measurements, one from either side of the spectrum;

3. The one-sided spectrum with the greatest signal-to-noise ratio (SNR), of at least 10 dB, was chosen as the candidate spectrum for the current component estimation; and

4. A moment calculation was performed by weighting the frequency components in the signal window of the candidate spectrum with the SNR values to estimate the central peak frequency. The SNR values for each point used in the weighting had to survive the minimum SNR threshold of 10 dB.

The spectra from each radar cell was subjected to the above procedure to generate polar grids of radial current data for each radar dataset. A sample plot of one of these grids in shown in Figure 4.1. For display purposes each point on the grid is averaged over a polar sector of 20 km in range and 10° in azimuth.

---

period. However, inexplicable results from the data analysis may require revisiting this assumption.

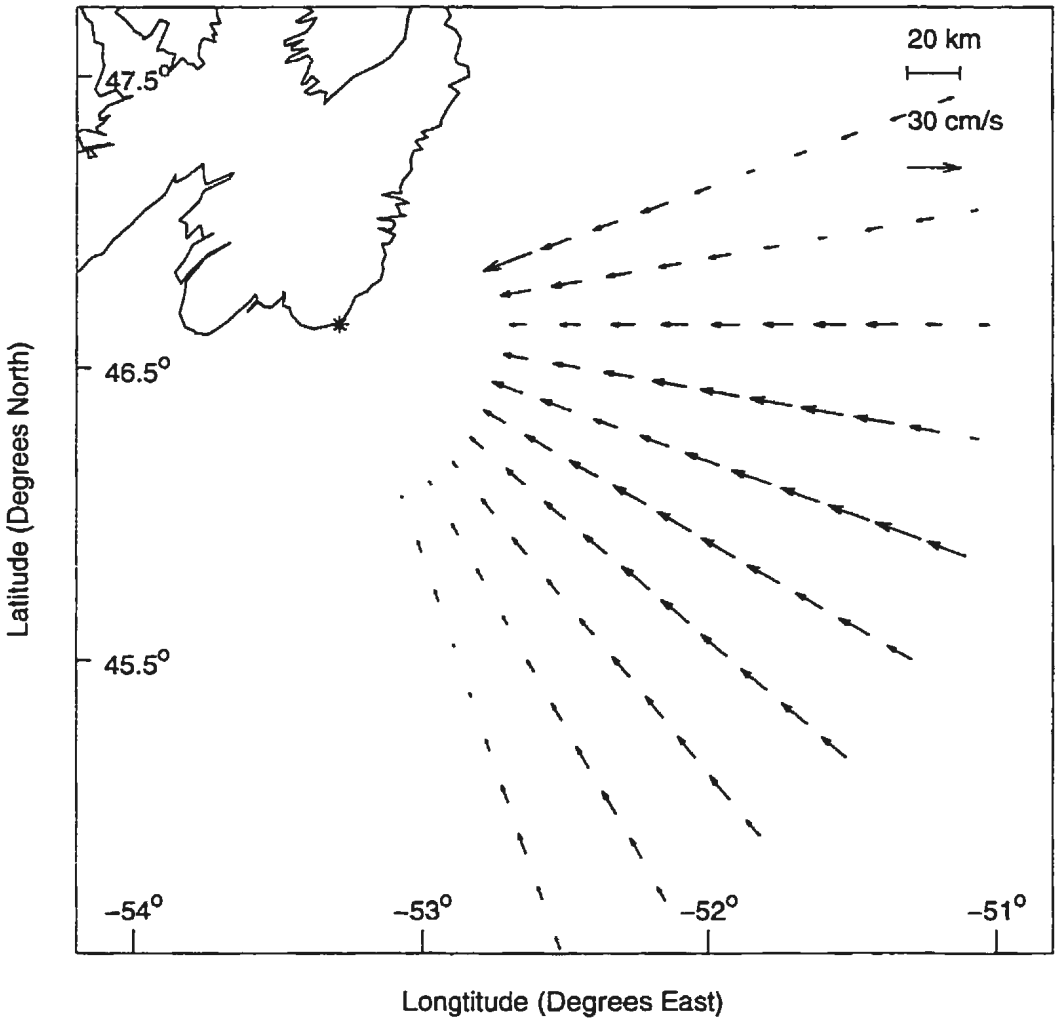

Figure 4.1: Radial current map processed from radar data collected on Oct 21,1992 at 11:53, NST. Note the wind-driven surface current flow is predominantly landward in this example.

4.4 Simulations

A simulation study was undertaken to estimate an approximate error bound on the radar and drifter current comparisons, based on the estimated errors of both techniques. This was performed for the direct radial and the vector current comparisons to: (1) test the software modules used in the data analysis procedures; and (2) to aid in the analysis of the actual radar data in the event that anomalous results were obtained.

For the direct radial component comparison (see Section 2.2.2) these errors can be

modelled, since they are known quantities. For example, the estimated radar error per radar cell is $\approx \pm 3.5$ cm/s while the drifter error is $\approx \pm 6$ cm/s (Helbig [49]). Hence, a comparison could be simulated and used as a benchmark for the actual radial component comparison. In this way the statistics from a comparison of the simulated and the real data should agree if the errors were properly modelled. The vector current algorithmn could also be tested using a similar scenario. Since this algorithm assumes a uniform current about a test position on the ocean surface, the generation of this current could be simulated from any current which was assumed to prevail at the point, and in the vicinity of the point. Moreover, by extending the region over which the benchmark current is assumed to exist, both the radial and the vector current algorithmn can be tested with the same simulated datasets.

The radar test data, which emulated a time sequence of actual radial current grids, were simulated assuming the existence of a spatially uniform current field about a position of comparison in the coverage zone from each radial map. This was deemed adequate for the direct radial component comparison since these positions would be representative of an actual radar/drifter test point. In other words, the same radial component should essentially be estimated using either the radar or drifter current estimate. For the application of the vector current algorithmn this may not be the case since the actual current data may deviate from the uniform test current estimate, as the distance from the test position increases. However, for the simulations, good agreement is expected since the assumption of current uniformity is enforced by the prevailing test current. By using this approach the statistics of the simulation results, and the actual data, should be similar if the actual current was indeed uniform. This may also provide some insight in detecting non-uniform current regions.

Since the drifter data is considered to be the sea-truthed dataset for this comparison, currents estimated from this data were chosen as the test or benchmark current. For both the radar and drifter simulated datasets, the actual drifter estimate at the

midpoint of a radar data collection, in time, was taken to be the test current. However, the errors associated with this drifter estimated current are known to exhibit Gaussian standard errors from $5-7$ cm/s. To simulate this error range, random normal deviates from a uniform distribution over this interval were added to the drifter current components. For example, if the output from a random uniform number generator on the above error interval was 5.5 cm/s, then this would be the standard error of the Gaussian random variable. This is the thrust of the current simulations for the drifter components. For the radar simulation the benchmark current was held constant for the duration of an actual radar data collection. The current was projected on each of the radar beam directions used to process the actual radar data. This step yielded a set of noiseless radar radial velocity data. Since it is has been shown that surface current radial velocities are Gaussian random variables (Barrick and Snider [51]), the noiseless data was smeared with a random normal deviate. The standard error of this random variable was chosen to be 1/2 the current resolution of an FFT frequency bin, or approximately 3.5 cm/s (See Section's 2.2.2 and 4.3). All the radar datasets are used in this manner to generate a simulated version of the actual radar data.

4.5 Direct Radial Radar/Drifter Comparison

At each point of comparison a radar estimate was obtained by averaging the radial components within a radius of 2.4 km from the location of the drifter current estimate. Since the radar range resolution was 0.4 km, approximately 12 range cells along the radial direction were used in the averaging process. For example, at ranges of 50, 100 and 150 kms an arclength of 4.8 km, subtends angles of approximately 6°, 3° and 2°, respectively. Therefore, at 50 and 150 kms approximately 24 and 12 points, respectively, were used to compute the mean radial current from a region with a surface area of approximately 20 square kms.

Since the drifter estimates were constrained to three hour intervals, a linear interpolation of the drifter estimate was required if the radar time did not coincide with one of these intervals.

To illustrate the effect of SNR on the comparison, the radar data were processed using two SNR values of 10 and 30 dB.[3] The 10 dB case was studied to determine if this minimum SNR case was sufficient for radial current estimation. In contrast to this, the 30 dB case was considered to determine if the data comparison is improved by using a relatively high SNR criteria. Since all three drifter datasets were used in this comparison, this yielded a total of six radial component comparisons. These were subsequently analysed, using a simple linear regression, to estimate the correlation between the sea-truthed radial currents estimated from the drifter data and those estimates provided by the radar technique.

[3]See Section 4.3 for a discussion of how these SNR values were computed from the radar spectra.

4.6 Vector Surface Current Estimation

4.6.1 Introduction

The performance of the vector surface current estimation algorithmn will first be addressed using the known test radial current data as described in Section 4.4. These simulated fields of radial current grids will form the basic test vectors for the algorithmn. Ideally the test data set should mimic the actual data with simulations based on some surface current model parameters. However, this poses a problem since the actual data is a function of the essentially unknown current regime. The only known quantities are the current estimates from the three drifter tracks. Therefore the extent of the test data for the algorithmn is based on the current simulations from the known drifter velocities.

The purpose of the simulations was for software testing and not for establishing a robust radar signal simulation. This could be quite complex for a HF system if the uncertainties propagating throughout the radar system were calculated, starting from the raw voltages measured at the antenna system to the output radar spectra (Lipa and Barrick [17], Lipa and Barrick [52]). Since a robust radar signal simulation is beyond the scope of this thesis, for the sake of simplicity uncertainties were simulated in the resultant spectra as an error in the radial current estimate. As already mentioned in Section 4.4, the radial component of the reference current estimated from the drifter data was projected along each radar beam direction used in the actual radar datasets to simulate a uniform current field for each set. Error estimates were computed from knowing the Gaussian statistics of the radar current estimate. The simulated radial current data were then processed by the algorithmn to crudely determine its stability for varying algorithmn parameters. Finally, the algorithmn was subjected to the actual radar data with a subsequent comparison to the actual drifter velocities.

4.6.2 Selection of Algorithmn Parameters

For a single vector current estimate, radial current speeds from a polar sector of radar data are required, namely a Q-type sector as discussed in Section 2.3.1. However, determining the optimal size of this sector by specifying the values of ΔR and $\Delta\Theta$ has been an arbitrary aspect of the procedure at this stage. The emphasis has been on algorithmn correctness as opposed to optimization. In other words, algorithmn performance in the presence of a uniform current with added noise is the primary objective of this exercise. At this stage of the algorithm development this is the simplest approach, since we wish to provide a comparative analysis between the radar and drifter methods with the assumption the drifter estimate is representative of the current in a Q-type sector in the vicinity of this estimate. However, it is possible that the oceanographic regimes about the drifter estimate and the polar radar sector may not be the same. Since the algorithmn requires, as input, radar data from a region which may be larger than the region represented by the drifter estimate, it is unclear how the effects of a non-uniform current may bias the results. In the worst case scenario it is hoped the current estimate is indicative of the mean current in the region of interest. The problems associated with a comparison of this nature will be discussed in the following section.

4.6.3 Algorithmn Constraints

To perform a definitive comparison between the radar and drifter estimates, the oceanographic regimes associated with both estimates should coincide. This presents a problem when the polar sector used by the vector current algorithmn is significantly larger than the region in the vicinity of a drifter estimate. To apply the algorithmn we are assuming the current is uniform in the sector. However, this may be true for only a small region about the drifter position. Ideally, this region should span some portion of the drifter track. It should also be as small as possible, such that the radar

vector current estimate is not distorted by radial components far removed from the position of the drifter estimate.

As the polar sector size is reduced the concerns noted in the above paragraph do not exist or are not as prominent. However, there are other issues to consider when this situation arises and these are a function of the radar's spatial parameters. For example, the angular extent of the sector, $\Delta\Theta$, used by the vector current algorithm, will be affected by the number of beams required to span it. This may adversely affect the tangential component estimate if the ratio of this parameter to the radar beamwidth is not greater than two. This is apparent from inspecting the general formulation equations in Section 2.3.1, since at least two beams must span the region for the solution to be unique. This effect is even more pronounced if the spectral resolution, and hence the current resolution, is too coarse to sense the radial current change from beam to beam.

The other extreme case is when the region size becomes too large. In this case, errors in estimating the tangential current may be due to unknown current variation throughout the region. In other words, the point estimate provided by the drifter data does not adequately represent the mean current of the region.

For a consistent comparison each radar estimate should be computed using data from a constant region size for each radar/drifter estimate. This will avoid any bias as a result of variable spatial averaging in a comparison dataset. For example, the radar estimate from a sector of a hundred square kilometers will consist of more range-azimuth cells, and hence more regression points, than an estimate from a few square kilometers. The validity of such a comparison holds only if the same current exists over both regions.

Due to the inherent polar nature of the radar data, the radial point density is a function of range in that fewer points are available per unit area as the range is increased. This is a result of the beamwidth of a directional antenna, since the arc

subtended by the beam increases in size with range resulting in a larger radar cell size per fixed range resolution and beamwidth. This would not be a problem if the antenna beamwidth was a 'pencil' beam, since it could be steered in any direction to obtain the desired radial current density per unit area. However, with a fixed beamwidth from an actual system only one radial current speed is estimated from each range-azimuth cell, and this cell grows in size with increasing range. At ranges of 50, 100 and 200 km, for example, a beamwidth of 5° subtends, in azimuth, a distance of 4.4, 8.7 and 17.4 km respectively. If the radial extent of the input data is 5 km and data from three adjacent beams are used to estimate the current components, the region sizes corresponding to these ranges and beamwidth will be 66, 130 and 260 square kilometers respectively. In order to maintain constant-area sectors, an alternative approach would be to permit the radial width of the cell to proportionately decrease as the range is increased. However, the shape of the sectors will exhibit a range dependency in that the sectors becomes 'thinner' as the range is increased. As well, there is still no guarantee that current uniformity will prevail even in this situation since the region, instead of being modified radially, will be extended in a lateral sense. Therefore, when comparing estimates at different ranges, this aspect of the current processing scheme will ultimately have to be addressed.

The azimuth extent used by the vector current algorithmn must take into consideration the receive antenna beamwidth in the direction of the location of the estimate. For example, as noted in Section 3.2.1, the radar beamwidth of the Cape Race system is approximately 6° when the beam is steered 60° from broadside. Therefore, when performing an estimate near the azimuthal extremes of the radar coverage zone care must be taken to ensure that this extent is large enough to at least cover two beams in the estimate sector. Moreover, if the current resolution of the datasets is coarse, as compared to the mean currents of the coverage area, additional care must be taken such that the change in radial current over azimuth is adequate to sense

the tangential component. For example, the radar data used here were processed to yield a current resolution of approximately 7 cm/s, while the mean current over the experimental zone is on the order of 20 cm/s. Therefore, it may be difficult to measure the change in the radial current from adjacent beams, and hence the tangential current component, if the change is less than the nominal error of the radial current measurement. An alternative in this case is to increase the azimuthal extent of the region and proceed with the assumption of current uniformity.

In summary, from the above discussion there is a clear tradeoff between the radar parameters of beamwidth and current resolution, as well as the selection of the optimal region size to be used for vector current estimation based on these parameters. This will also depend on the variability of the current regimes being monitored and the magnitudes of the currents. For example, the technique may provide better estimates when currents are large, relative to the current resolution of the system. It may also provide reliable mean current estimates in the event of extreme current variability in the estimation region if the size chosen is large enough to 'force' a mean estimate from the region. All in all, many of the points noted here will have to be investigated further to determine their effects on the reliability of the estimate provided by the algorithmn.

4.6.4 Simplifications

At this stage in the algorithmn development, it is unclear how the main algorithmn parameters, ΔR and $\Delta\Theta$, affect the solution. It may ultimately require some 'goodness of fit' testing while varying the algorithmn parameters to minimize the solution in a least squares sense with some optimal set. Since this may detract from the fundamental issue of establishing the potential of the algorithmn for current estimation, optimal parameter selection will not be dealt with. Hence, for the sake of simplicity, key issues related to the algorithmn fundamentals will be addressed here. These will

simplify the analysis by converting this multi-parameter model to a simpler and more intuitive form.

To begin this simplification process, consider the general formulation equations presented in Section 2.3.1. In this formulation V_x can be equated to V_r, the radial component in the sector, while V_y becomes V_t, the tangential component. This can easily be shown by an appropriate axis rotation. By setting the radial component to an arbitrary constant it is clear that the tangential component is a function of the changing radial components measured by the radar. Even though this may be intuitive, this step reveals the key parameter in the tangential estimation process: the linear change in the radial current variation over azimuth. Hence, using this approach, an investigation of the effect of this variable only will be considered. This simplification allows us to consider the effect of the variation of azimuth only. As the radial extent is held constant the effect of that variable should be minimized with respect to the azimuthal variation.

With this simplification, the variability of results is studied using three azimuthal extents. The range increment was held constant at the arclength used for the direct radial component averaging, 4.8 km, while the angular extents were chosen as 12°, 20° and 36° (i.e. an odd integral number of nominal radar beamwidths). For each case the point density is preserved, in that radial data from each radar cell contains only one radial component at any range while the sector area is increasing with range. In other words, for each angular extent the same number of radial components will be used to estimate the vector current at each estimation point. However, this may not be the optimal approach, as mentioned in the previous section, since this does not preserve area. At ranges of 50 and 200 km, the area coverage is approximately 50 and 200 square kilometers, respectively, for the 12° case. For the 36° case this corresponds to areas of 150 and 600 square kilometers. An illustration of the size of these regions with respect to the radar coverage area is shown in Figure 4.2.

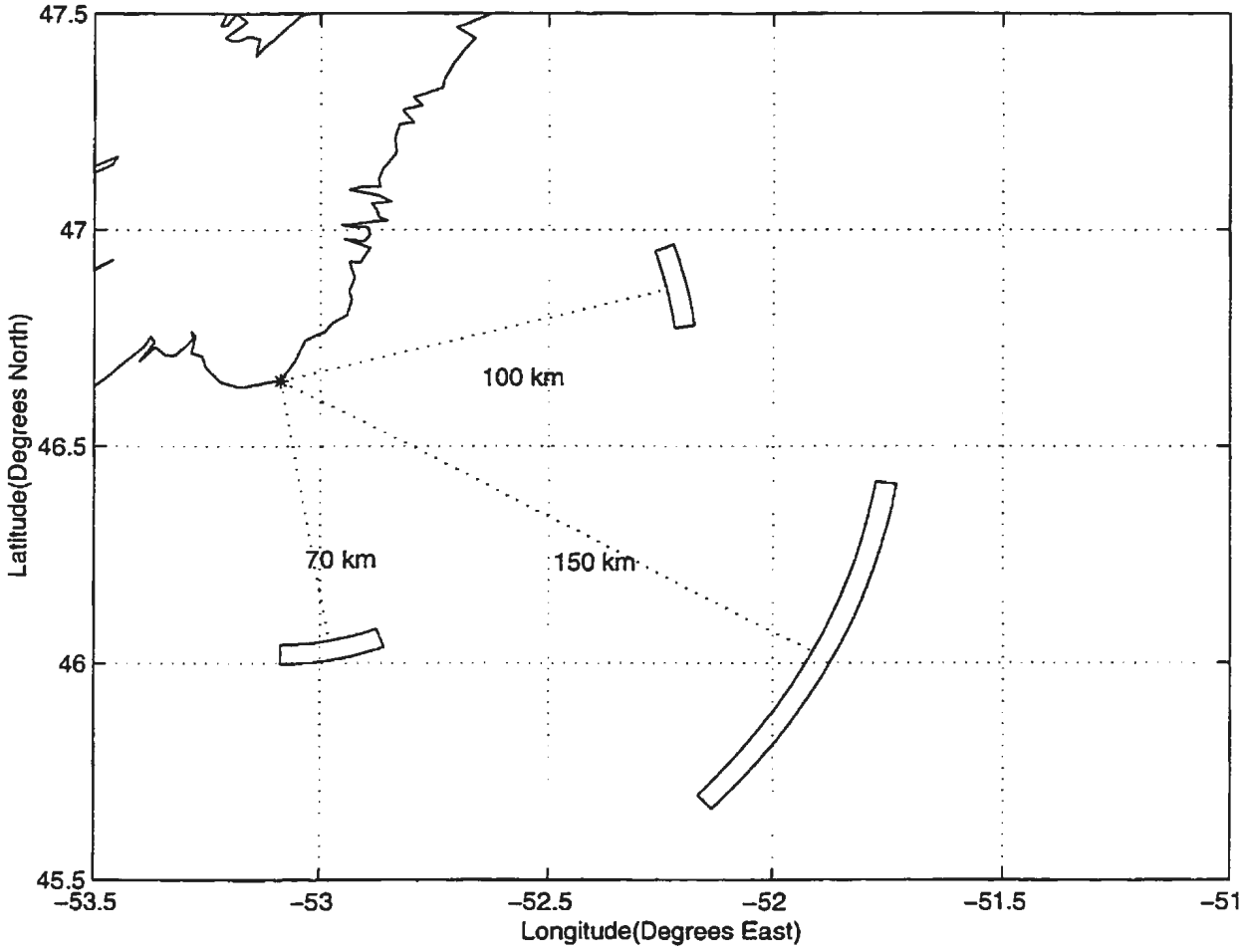

Figure 4.2: Typical polar sectors used for vector current estimation

4.6.5 Data Reduction

The experimental data were processed to yield a polar grid resolution of 1° and 400 meters along the azimuth and radial directions, respectively. This data was subsequently averaged to yield a resultant grid resolution of 4° by 1.2 km. This step was performed, firstly, to adhere to the nominal radar beamwidth (i.e. 4°) and, secondly, to reduce the variability of the radial current estimate over range. These steps were also necessary to reduce the computational load on the software module which computes the current components. These new values correspond to the the parameters $\Delta\theta$ and Δr, respectively, as discussed in Chapter 2. In this case, however, Δr is the range resolution of the new grid (i.e. 1.2 km). The corresponding values

for the n beams is therefore 3, 5 and 9 for the 12°, 20° and 36° cases, respectively. The number of effective range cells, m, is 4.

4.6.6 Processing

The output from the data reduction step was processed for vector currents using the three region sizes defined in the previous section. The central position of this region coincided with the position where a drifter estimate was computed. Hence, for each drifter position used in the comparison, 12, 20 and 36 input data points were available for the regression algorithmn. Each of the points, which comprised the sectors, also had to meet the SNR criteria of at least 10 dB to be considered as valid. If this resulted in any missing data points in a sector, or 'holes', which did not meet the SNR criteria, the estimate computed from the sector was not used in the comparison. A regression analysis was then applied to the drifter and radar computed current components in order to study the correlation between the two estimates.

Chapter 5

Results and Discussion

5.1 Introduction

The results from the application of the data analysis procedures outlined in Chapter 4 are presented and discussed. These are partitioned as two distinct sections, one for the direct radial and one for the vector current comparisons.

The results from the direct radial surface current comparison are presented in the first section of this chapter. This is the fundamental comparison since it illustrates the radar's ability to directly monitor the radial component of the surface current in the vicinity of a drifter estimate. The results presented are from the analysis of the three drifter/radar datasets, both simulated and actual.

Next, the results from the vector surface current algorithm are presented. However, it was not deemed necessary to provide a comparison from all three drifter datasets, as was done in the direct radial current comparison, since comparisons showing both current components, with varying algorithm parameters, would only clutter the thesis with redundant graphs and tables. Since an illustration of the potential of the algorithm for vector surface current estimation is one of the goals of this demonstration, data from only buoy 3 was used in the comparison study, as it provided the most radar/drifter comparisons.

For ease of presentation, the comparisons are presented as scattergrams and associated tables illustrating the statistics of the comparison. The statistics associated

with the graphs are from a linear regression used to summarize the results of the analysis. Since the drifter and radar current estimates are not strictly equivalent random variables (See Section 4.2) these statistical tables are only intended to illustrate any gross inconsistencies in the analysis results.

A brief discussion on the results from the comparisons, including possible anomalies in the investigation, will also be presented.

5.2 Direct Radial Surface Current Comparison

5.2.1 Simulations

One set of the results from the simulations, in the form of scattergrams, is shown in Figure 5.1. In these scattergrams the minimum SNR criteria for the simulated radar data was 30 dB. In other words, only Bragg spectral components which met this criteria were used in the mean radar estimate (See Sections 4.3 and 4.5). A summary

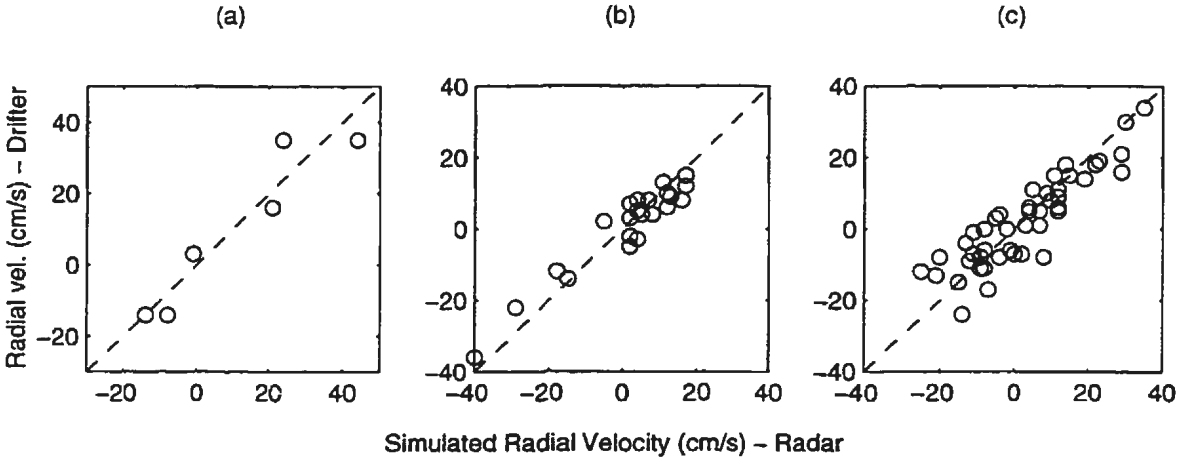

Figure 5.1: Scattergrams of simulated radial surface currents of drifter versus radar estimates for 30 dB case. (a) , (b) and (c) correspond to simulations from data generated from Buoys 1, 2 and 3, respectively.

of the statistical analysis of the radial component comparisons from the simulations is shown in Table 5.1.

Track #	Radial Currents from Simulations (cm/s)					$y = a_o + a_1 x$		r	Num. of
	x =Radar		y =Drifter						
	$\bar{x}$	σ_x	$\bar{y}$	σ_y	s	a_o	a_1	Corr. Coef.	Pts.
1	10.17	22.30	11.00	22.31	8.17	1.39	0.94	0.95	6
2	1.30	12.22	1.87	14.60	4.42	0.38	1.14	0.96	23
3	2.13	12.50	2.70	14.42	6.59	0.51	1.03	0.89	48

Table 5.1: Summary of statistical comparison of simulated current components using an SNR of 30 dB. The mean and standard deviations of the three datasets are denoted by $\bar{}$ and σ, respectively, and the standard deviation of the regression of y on x is labelled s.

The combined results [1] from the simulations indicate that all measurements fall within approximately ± 6 cm/s of each other, which is within the estimated errors of the buoy and radar measurements. For the combined cases, 83% of the total variation in the radial components is explained by the regression.

5.2.2 Real Data

Figures 5.3 and 5.4 display the time series of the buoy radial velocity, together with the radar point estimates and their standard errors. Considering the variation of the drifter-derived current components over time it is quite remarkable that the radar so closely imitated this trend.

A sample of the results, in the form of scattergrams, illustrating the performance of the radar using an SNR value of 30 dB, is shown in Figure 5.2. A statistical summary of the regression for each individual case in shown in Table 5.2 for both SNR studies. The scatter between radar- and buoy-derived estimates of the radial surface current was within the estimated error bounds of both techniques. This is in close agreement with the simulated results, thereby giving credibility to the simulation technique.

[1] Used in this context, "combined" refers to the results where the points from all three cases are used in the regression. This is computed to give a comparitive estimate of the correlation coefficient and the standard error from the overall analysis.

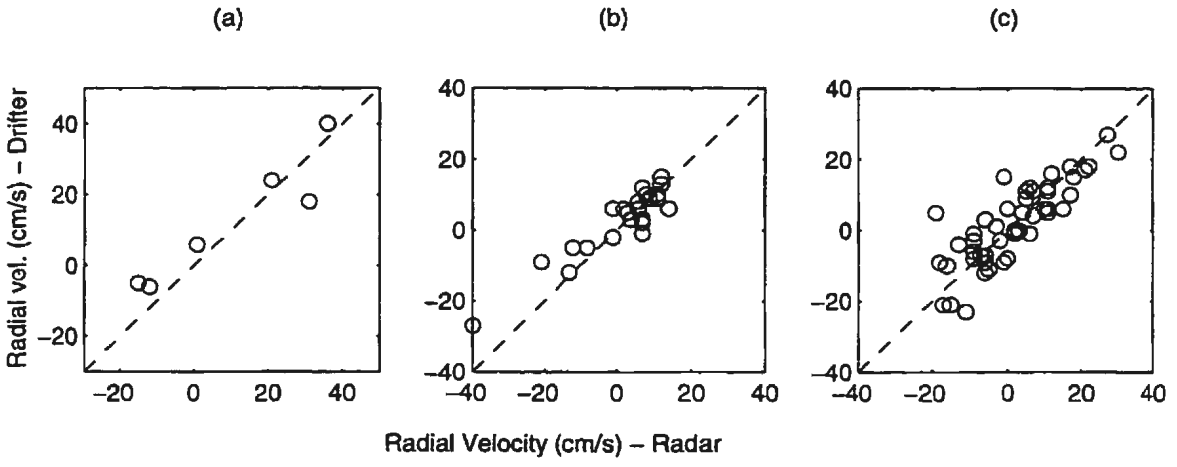

Figure 5.2: Scattergrams of radial surface currents of drifter versus radar estimates using real data; (a) , (b) and (c) correspond to Buoys 1, 2 and 3 respectively.

Track #	Radial Currents Using Real Data (cm/s)					$y = a_o + a_1 x$		r	Num. of
	x =Radar		y =Drifter						
	$\bar{x}$	σ_x	$\bar{y}$	σ_y	s	a_o	a_1	Corr. Coef.	Pts.
1	12.83	17.94	10.33	22.03	8.34	-4.50	1.16	0.94	6
2	2.61	9.50	1.30	12.70	4.96	-1.92	1.24	0.92	23
3	2.48	11.26	2.15	12.08	6.79	-0.07	0.89	0.83	48

(1)

Track #	Radial Currents Using Real Data (cm/s)					$y = a_o + a_1 x$		r	Num. of
	x =Radar		y =Drifter						
	$\bar{x}$	σ_x	$\bar{y}$	σ_y	s	a_o	a_1	Corr. Coef.	Pts.
1	12.83	17.94	10.33	22.03	8.34	-4.50	1.16	0.94	6
2	2.70	9.53	1.30	12.70	4.91	-2.02	1.23	0.93	23
3	2.27	11.44	2.15	12.08	6.77	0.15	0.88	0.83	48

(2)

Table 5.2: Summary of statistical comparison of radial current components using real data with (1) 10 dB SNR and (2) 30 dB SNR. The mean and standard deviations of the three datasets are denoted by $\bar{}$ and σ, respectively, and the standard deviation of the regression of y on x is labelled s.

The combined results show nearly all measurements fall within approximately ±6.5 cm/s of each other, which is within the estimated standard deviation of the buoy and radar measurements. The correlation coefficient, for the same, indicates that 76% of the total variation in the radial components is explained by the regression.

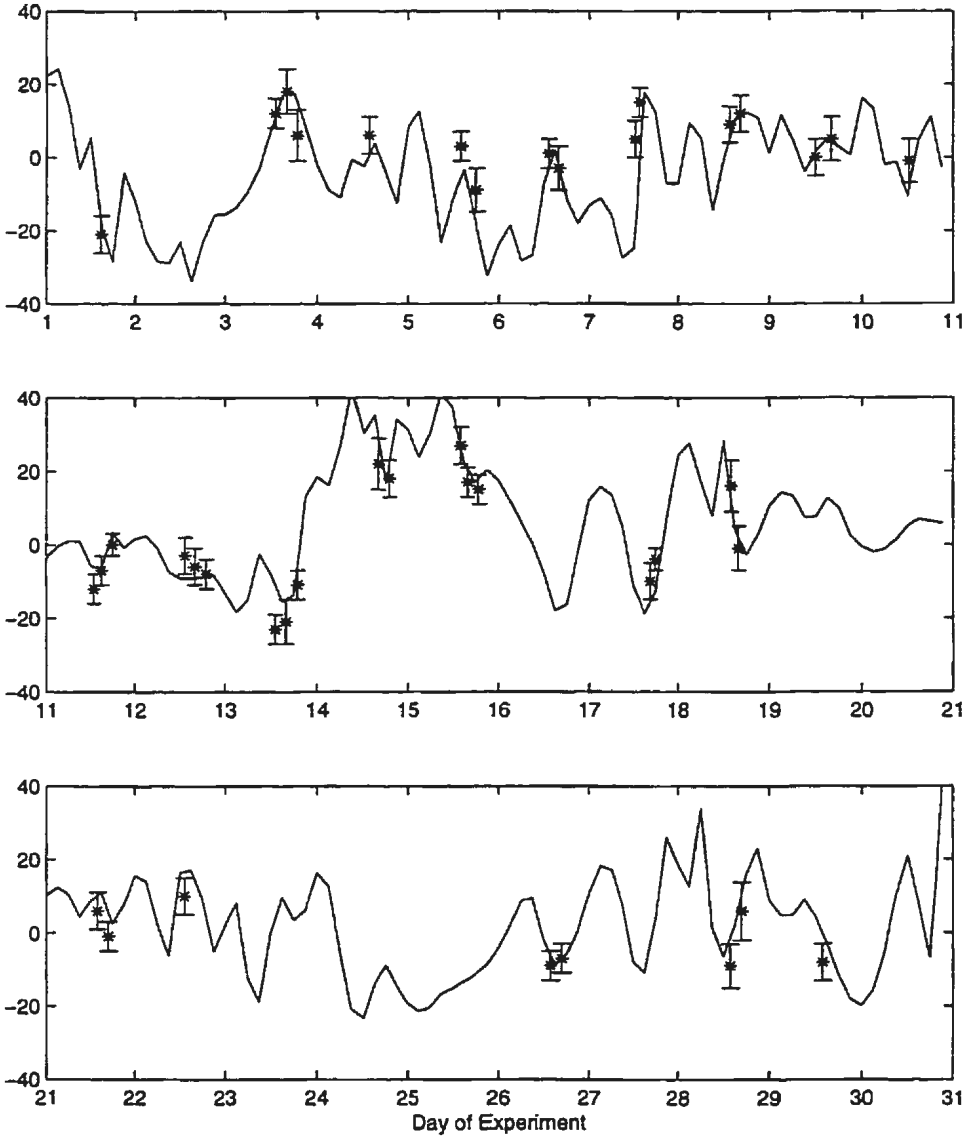

Figure 5.3: Comparison of currents estimated from Buoy 3 (solid line) and error-barred radar data (*)

The slight differences in the standard error and the correlation coefficients in the simulated and actual results can be attributed to the way the radar and drifter sense the current, as described in Section 4.2. It is apparent from the results presented in

Table 5.2 that the SNR cases of 10 dB and 30 dB are statistically equivalent. Hence, an SNR of 10 dB may be sufficient for the estimation of the radial currents from radar data collected during day-time operation. Since these values were obtained

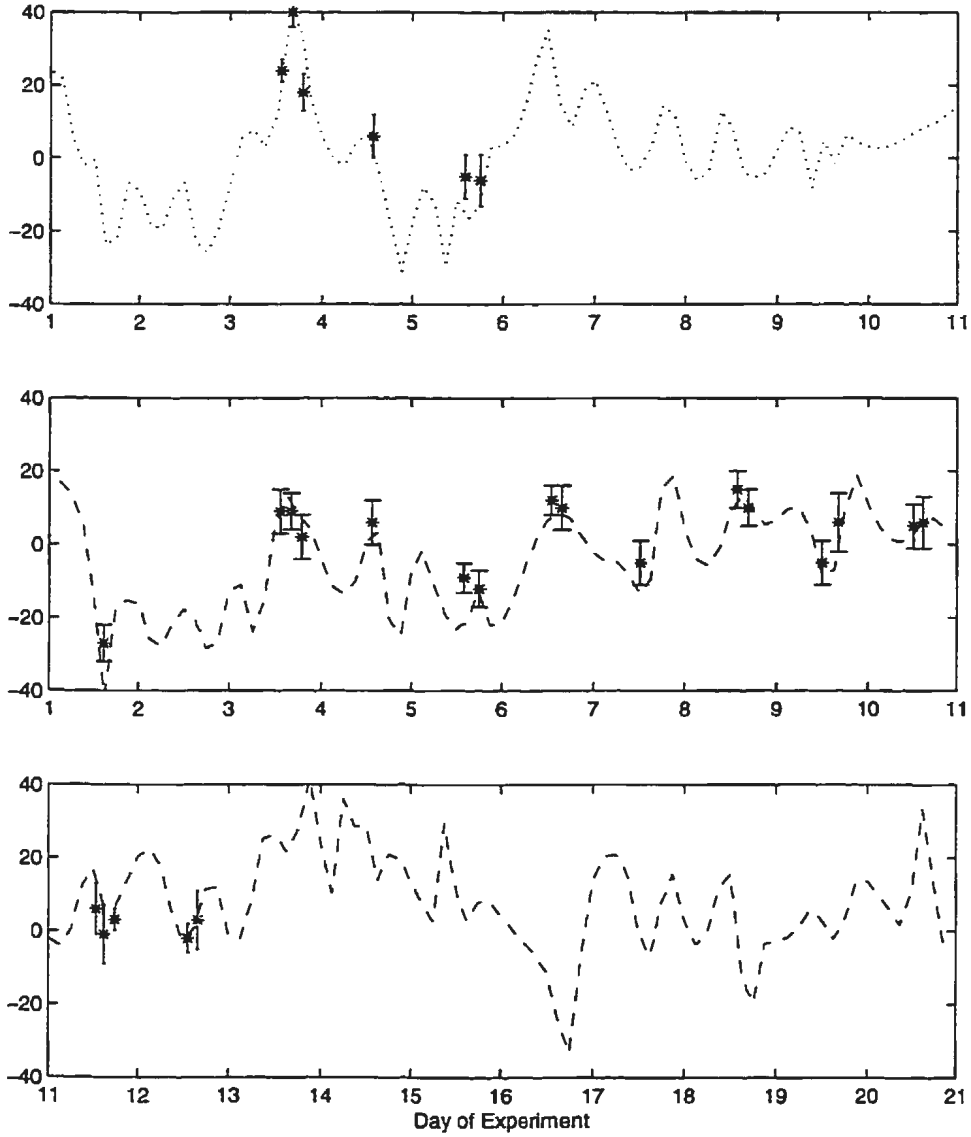

Figure 5.4: Comparison of currents estimated from Buoys 1 (dotted line) and 2 (dashed line) and the error-barred radar data (*).

over a wide variety of oceanic conditions, as is clear from the wind data appearing in Figure 5.5, it is apparent that the results were independent of the sea state conditions experienced.

Prior investigations have provided evidence of discrepancies in radar-derived cur-

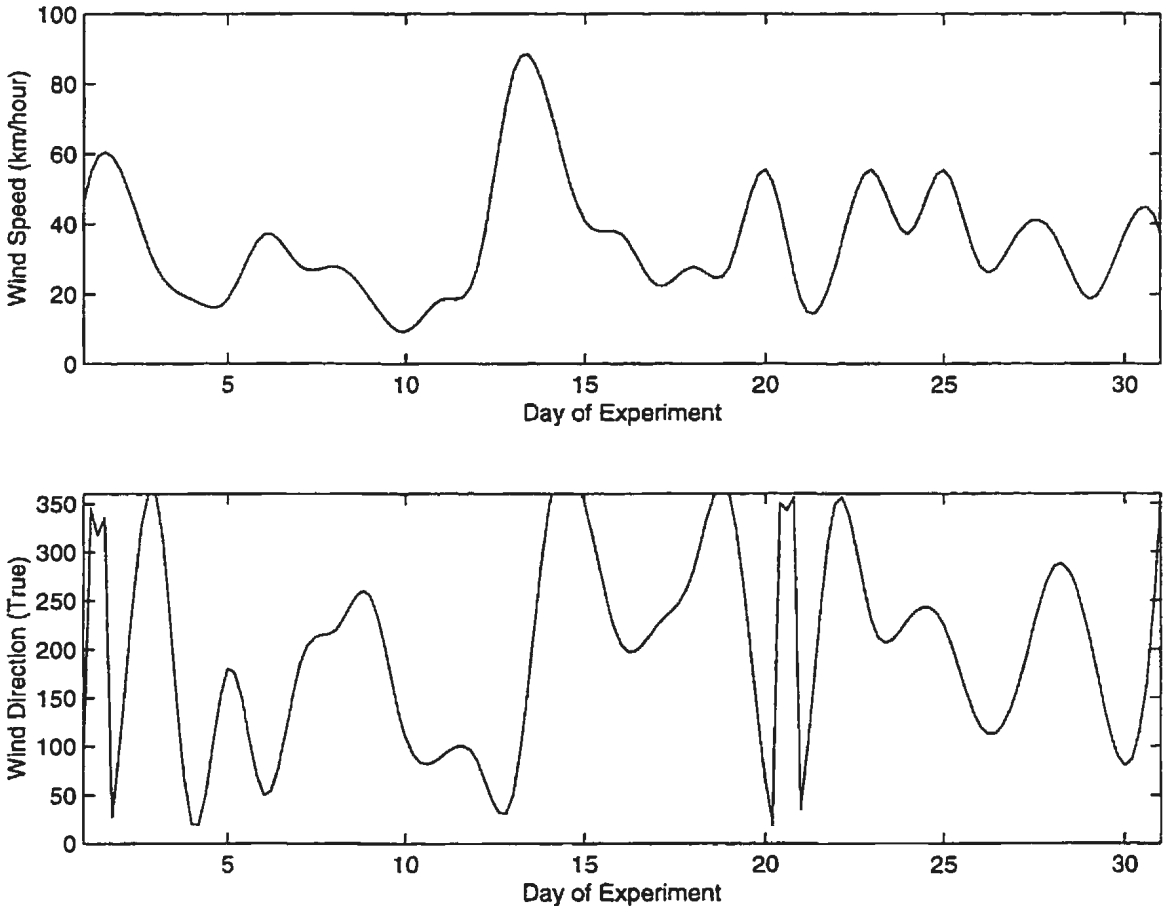

Figure 5.5: Wind velocities for position 45° 14′ N and 52° 18′ W during the experimental period

rents when wind and tide are in opposite directions (Lawrence and Smith [30]) and when current shear, coincident with wind reversals, occurs (Essen *et al.* [34]). However, in this case there was no evidence that these conditions were present when the buoys were being interrogated by the satellite. If they did exist, they were not observed in the comparison. Thus, anomalies observed by Lawrence and Smith [30] and Essen et al. [34] may have resulted from the fact that, in the experiments cited, current meters provided groundtruthing. The current meters were moored at depths well below the $\lambda_0/4\pi$ layer, to which the radar measurements are sensitive, while the drifters used in the experiment related to this thesis responded to about the top metre of ocean. Another factor which might be expected to cause discrepancies in

measurements delivered by radar and buoys is their temporal sampling difference. A relatively small CIT, typically six minutes, is used to obtain a point radar current measurement. The corresponding drifter estimate, which is obtained from spline fitting and discrete time differentiating the satellite deduced drifter tracks, may result in a 'smoother' result. This may be more pronounced since approximately 10 positions per day were typically recorded from the ARGOS satellite system. Here again, however, there is no obvious indication of results being affected significantly by this possibility. One explanation for this observation was that the current regime was uniform for a period of several hours, or many radar data collection intervals.

5.3 Vector Surface Currents

Current components estimated from the track of drifter buoy 3 were compared to those estimated from the vector current algorithm. Three cases were studied to illustrate the performance of the vector current algorithm. Each case used a constant angular span of 12°, 20°, and 36°, respectively, while the other two parameters, Δr and ΔR, were set to 1.2 and 4.8 km, respectively (See Sections 2.3.1, 4.6.4, and 4.6.5). Simulated and actual data are compared, using both current components, to yield 12 intercomparisons, or six for each component.

5.3.1 Simulations

The results, in the form of scattergrams illustrating the performance of the vector current algorithm in estimating both current components using simulated data, are shown in Figure 5.6.

Table 5.3 shows a summary of the statistical analysis of the results of the simulations.

5.3.1.1 Radial Component

The algorithm produces estimates which are comparable with those obtained from the direct radial component simulations. The regression errors are of the same order of magnitude, with values ranging from 4.54 to 6.65 cm/s. In the worst case, 77% of the total variation in the radial components is explained by the regression.

The results, from the three test cases, tend to suggest the mean radial component computed from the algorithm is not significantly affected by the azimuthal variation of the sector. This may be solely due to the small spatial radial current variability in the regions selected for processing. In other words, the mean radial component in the region should not be very different from the drifter-computed estimate since current uniformity was 'forced' into each sector of radial current data, input to the

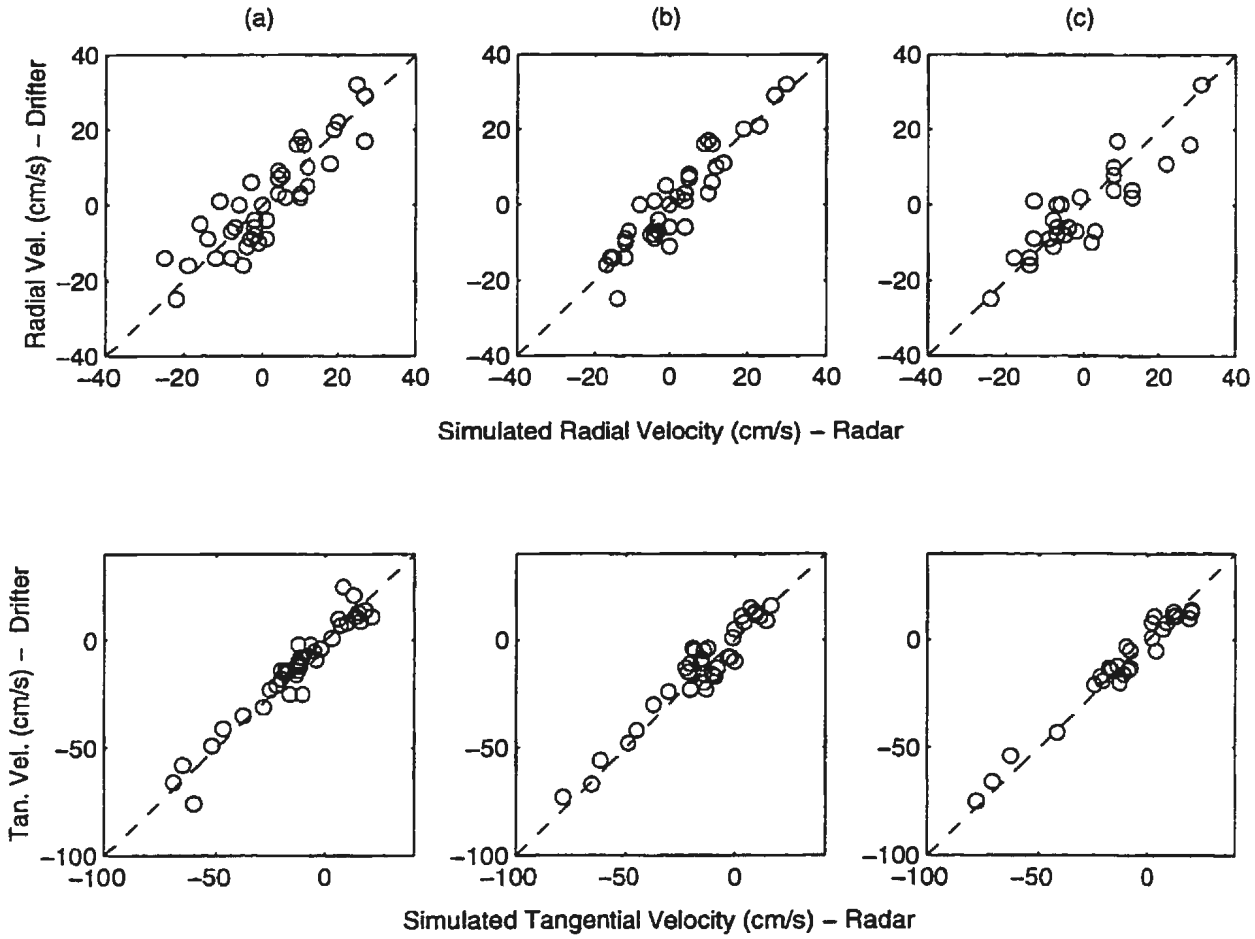

Figure 5.6: Scattergrams of simulated data results for vector currents for azimuth extents of (a) 12° (b) 20° (c) 36°

algorithm.

5.3.1.2 Tangential Component

There is a high degree of correlation within each comparison for the three cases studied, and the statistics are very similar as well. However, it is observed that an increase in the azimuthal extent of the sector results in an increase in the correlation coefficient as this extent is increased from 20° to 36°. In other words, a better fit to the data is obtained in the maximum angular extent case. One reason for this observation can be attributed to an increase in the range of the regression variable, $\Delta\Theta$, which leads to a more stable estimate of the current component as the range of

Case #	Radial Currents from Simulations (cm/s)					$y = a_o + a_1 x$		r Corr. Coef.	Num. of Pts.
	x =Radar		y =Drifter						
	$\bar{x}$	σ_x	$\bar{y}$	σ_y	s	a_o	a_1		
(1)	1.25	13.15	1.56	12.29	6.25	0.49	0.87	0.88	40
(2)	0.65	13.26	-0.97	13.43	4.54	-1.56	0.90	0.93	38
(3)	-1.68	11.84	0.04	12.63	6.65	1.55	0.90	0.88	28

Case #	Tangential Currents from Simulations (cm/s)					$y = a_o + a_1 x$		r Corr. Coef.	Num. of Pts.
	x =Radar		y =Drifter						
	$\bar{x}$	σ_x	$\bar{y}$	σ_y	s	a_o	a_1		
(1)	-12.68	22.57	-14.55	21.68	6.20	-3.09	0.90	0.96	40
(2)	-12.38	22.13	-12.86	22.26	6.44	-0.98	0.96	0.96	38
(3)	-10.89	23.77	-10.54	24.92	5.03	0.62	1.02	0.98	28

Table 5.3: Summary of statistical comparison of radial and tangential current components computed from the simulations. The mean and standard deviations of the three datasets are denoted by $\bar{}$ and σ, respectively, and the standard deviation of the regression of y on x is labelled s. Cases (1),(2) and (3) correspond to azimuthal extents of 12°, 20° and 36° respectively. This table summarizes the statistics associated with the scattergrams of Figure 5.6

the variable increases (Montgomery and Peck [53]). An analogy here is the difference in the slope error of a line estimated from a small number of 'closely spaced' points as opposed to a large number which are 'widely spaced'. In the worst case, 92% of the total variation seen in the tangential components is explained by the regression.

5.3.2 Real Data

Figure 5.7 displays the results of the performance of the algorithm, using real radar data, in the form of scattergrams. The graphs illustrate that the error in the tangential component estimate may be dependent on the angular extent of the sector. This was also observed in the simulated data examples. However, the variability of the scatter about the unity slope line for the tangential component estimates are quite different from the simulated examples.

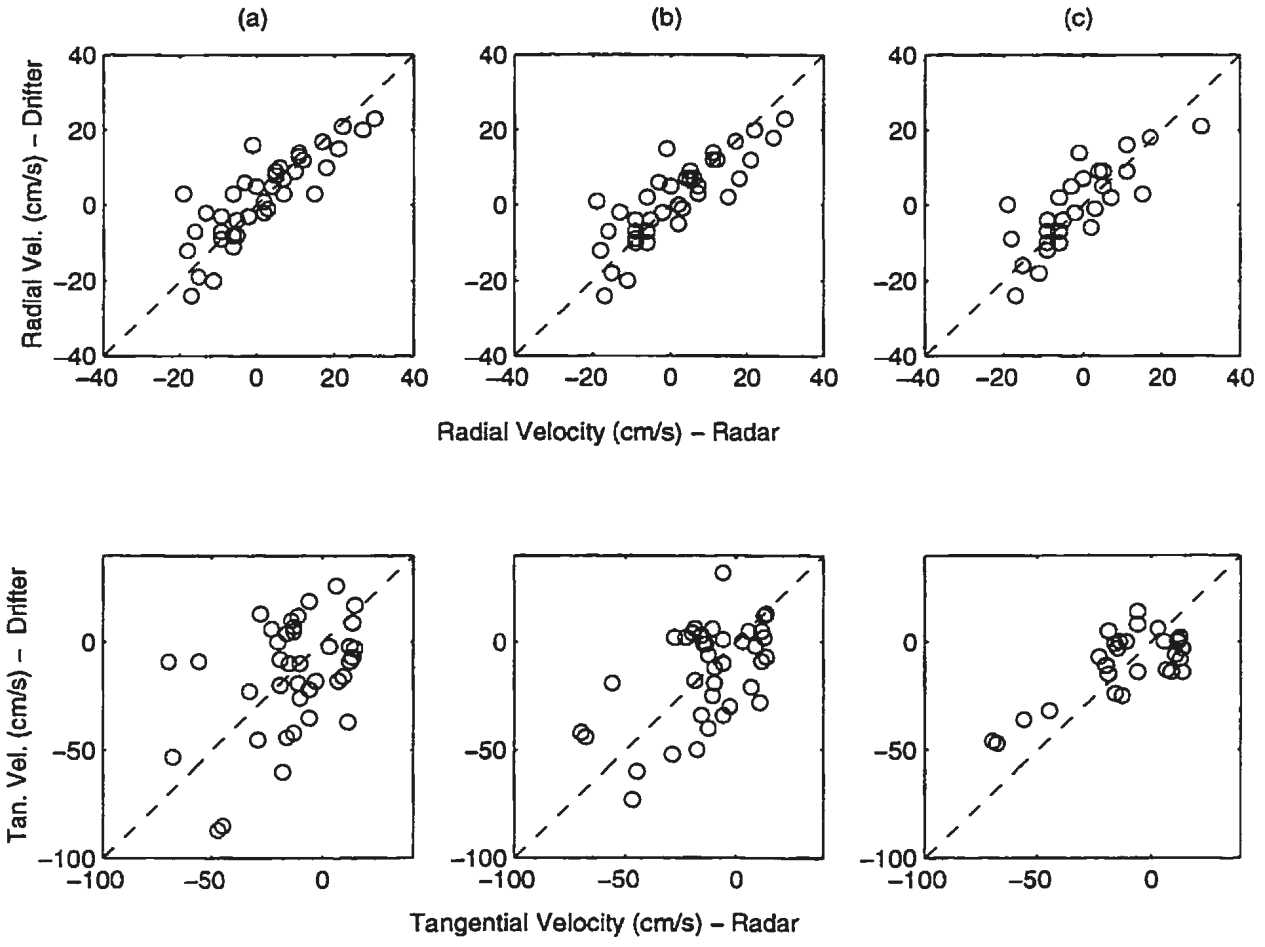

Figure 5.7: Scattergrams of vector current estimates using real radar and drifter data for azimuth extents of (a) 12° (b) 20° (c) 36°. Note the reduction in the standard error of the tangential component as the azimuthal extent is increased.

A statistical summary of the results of the actual data comparison is presented in Table 5.4.

5.3.2.1 Radial Component

The scattergrams suggest that the statistics from all three cases, as shown in Figure 5.7, are not signficantly different. This is also evidenced from the correlation coefficients, which range from 0.80 to 0.84, and the standard errors, which range from 6.94 to 7.22 cm/s.

The standard errors of the radial components estimated from the algorithm are not

Case #	Radial Currents from Real Data (cm/s)					$y = a_o + a_1 x$		r	Num. of
	x =Radar		y =Drifter		s			Corr. Coef.	Pts.
	$\bar{x}$	σ_x	$\bar{y}$	σ_y		a_o	a_1		
(1)	2.15	11.39	1.40	12.67	6.94	-0.61	0.93	0.84	40
(2)	1.63	11.17	1.34	12.88	7.22	-0.23	0.96	0.83	38
(3)	-0.36	11.10	-1.25	11.44	7.00	-0.96	0.82	0.80	28

Case #	Tangential Currents from Real Data (cm/s)					$y = a_o + a_1 x$		r	Num. of
	x =Radar		y =Drifter		s			Corr. Coef.	Pts.
	$\bar{x}$	σ_x	$\bar{y}$	σ_y		a_o	a_1		
(1)	-13.38	28.36	-13.35	21.43	19.80	-9.10	0.31	0.41	40
(2)	-14.32	23.05	-12.74	21.75	18.40	-5.29	0.52	0.55	38
(3)	-10.11	15.61	-11.04	24.01	16.51	0.44	1.14	0.74	28

Table 5.4: Summary of statistical comparison of radial and tangential current components computed from the actual radar data. The mean and standard deviations of the three datasets are denoted by $\bar{}$ and σ, respectively, and the standard deviation of the regression of y on x is labelled s. This table summarizes the statistics of the scattergrams presented in Figure 5.7

significantly different from the errors observed in the simulations, with a maximum mean difference of approximately 1 cm/s. This is also evident from inspecting the scattergrams for both cases. However, the correlation coefficients are lower and differ, in the worst case, by approximately 10 % from those of the simulations. The poorer fit, of the real data case, may be attributed to the differences between the radar and drifter current estimation mothods, as explained in Section 4.2, or due to non-uniform currents. The results indicate that at least 64 % of the variation in the radial components is explained by the regression. The corresponding quantity for the vector current simulations is 77 %.

The results also suggest that the radial component estimates are not significantly effected by the change in angular extents. This tends to suggest that the result may be useful in estimating the mean radial components of sectors of arbitrary but reasonable

size. In other words, the algorithm may give reliable radial estimates for a variety of polar extents and these estimates may provide a measure for the actual mean radial current. However, since the actual mean current was unknown in each sector, this conclusion, based on the results from this small sample set, is only hypothetical.

An error of approximately 7 cm/s is observed for the radial component estimate obtained here while the direct radial component estimation error is approximately 6.5 cm/s. Even though one may not consider these differences to be statistically significant, the slightly larger error in the vector algorithm result is probably due to a radial estimate which is computed using radial data from variable region sizes, as compared to the fixed region of averaging used in the direct comparison method. As well, the drifter estimate may be different from the estimate computed here since the latter is a function of radial current data which are slightly distanced from the track.

Of note, the radial component estimate from the vector current method may be used as a measure of the quality of the tangential component estimate. For example, one would intuitively expect the estimate from this method to be positively correlated with the direct radial component measurement when the two methods are applied to data from the same oceanic region. Without this inherent correlation, the tangential estimate computed from the vector current technique may be suspect. In other words, the result may be due to radial current estimates within the sector that exhibited extreme variability or non-linear behaviour, with respect to magnitude, over azimuth.

5.3.2.2 Tangential Component

The correlation coefficients, for the three cases studied, increase along with the azimuthal extent of each sector and range from 0.41 to 0.74. Coincident with this observation is a decrease in the standard error of the tangential component estimate as the azimuth extent increases. However, the mean value of this regression error, of approximately 18 cm/s, is relatively large as compared to the standard devia-

tions of the mean drifter and radar values. Moreover, since this standard error is approximately three times larger than the corresponding error term observed in the simulations, there is no strong evidence to suggest that a good positive correlation exists between the tangential components estimated from the radar data and the corresponding drifter estimates. However, it may be noted that the scatter in the plots from these cases are not as randomly distributed as the preceding deduction suggests. From observing Figure 5.7, one notes that the points are evenly distributed about the line of unity slope, indicating a positive correlation, albeit with a large regression standard error relative to the standard deviations of the simulated radar and drifter tangential current estimates. There may be a number of reasons for this result. First of all, the large errors may indicate the current was not uniform over the sectors; a scenario that was not examined in this thesis. In this case, the results may be unpredictable since the nature of the current regime is unknown. However, if this was the case one may expect the radial current estimates from this technique and the direct radial component comparison to be uncorrelated. This was certainly not the case since the errors for both comparisons were on the order of 6.5 cm/s, which is within the error bounds of the radar and drifter techniques. Therefore, a contradiction is apparent with respect to this result. Secondly, it is plausible that the mean drifter tangential components were not adequately represented by the point drifter estimate. In other words, the actual tangential component exhibits a greater variability, both temporally and spatially, than the radial component. This is evident from Table 5.3 where the tangential component standard errors are approximately twice that of the radial's. Another explanation for the suspect tangential component comparison may be due to possible system problems which were undetected during the experimental period. For example, the beamforming accuracy of the system was never thoroughly investigated during the program period. [2] The beamforming sys-

[2]The measurement accuracy of the beamforming system was never precisely validated during the current trials because: (1) the small budget allocated to the program didn't allow for any elaborate

tem, which is a programmable feature of the radar, gives the radar it's directional receiving capabilities. Appropriate phasing of the received signal, at each antenna channel, is required for this purpose in order to achieve the required beamwidth and directivity. Any errors in this aspect of the processing may be due to malfunctioning of the beamforming units[3], software problems, or inadequate calibration data. However, these beamforming errors may not be severe enough to comtaminate the results of the direct radial component comparison. To understand why this is possible, an explanation is provided, as well as a simulation, to demonstrate the effects of beam direction errors on the radar's direct radial component estimate. To begin, one may define a beam direction error, as a function of the radar radial current estimate and error, to be given by

$$\Delta\alpha = \sin^{-1}(V_{error}/V_r)$$

where

$$V_{error} = \text{Radial velocity error of radar}$$

and

$$V_r = \text{Mean radial velocity estimate of radar}$$

This error may not significantly effect the direct radial component comparison if the actual radial components do not vary appreciably over the beam error range, $\Delta\alpha$. For example, let's consider the case where V_{error} is ≈ 4.0 cm/s, the FFT resolution error of the experimental radar data. If V_r is the expected maximum radial velocity of the current to be observed by any beam, then an angular beam error of $\approx \pm 6°$ is obtained when this velocity is set to 40 cm/s, or the maximum radial current observed during

testing of this capability; and (2) good agreement was observed in the radar/drifter radial current comparisons which were performed periodically throughout the experimental period. In other words, there was no apparent need to check the system in the first place.

[3]This type of malfunction was noted during the experimental period. However, system evaluation was only performed when obvious deterioration of system performance was observed which occurred when more than 1 unit was defective. These types of failures are noted in Appendix A.

the experimental trials. In other words, a beam angle error of this magnitude may not significantly effect the results of the direct radial velocity comparison since the 'sloppiness' of the beam is not detected in the end result (i.e. the radar estimate is still within the error limits of the radar and drifter current estimate techniques). Further, this beam error is a 'best case scenario' since currents are typically on the order of 20 cm/s in the region where most of the radar estimates from the experimental data used here where obtained which is in the area of the Avalon Channel. In other words, if current magnitudes are not significantly larger than the radar current error, these directional errors may be difficult to isolate upon inspection of a radar/drifter radial component comparison. The masking of these beam errors will be further illustrated by a simulation. In the simulation the beam errors are assumed to be Gaussian, with zero mean and having a standard deviation of 6°. This beam direction 'noise' was added to the actual radar radial data by shifting the bearing of the radar estimate, by this error angle term, to generate a beam-errored data set. A direct radial component comparison was then performed between the radial components of drifter buoy 3 and the beam-errored data. This example utilized the same analysis procedure which was used in Section 4.5. The results are shown in the scattergrams of Figure 5.8. It is evident, from inspection, that the difference in the scatter is not significantly affected by the beam errors used here. Therefore, for the current regime studied here, it is quite plausible to obtain a good comparison for the direct radial component estimate even with significant beam direction errors.

The effect of beamforming errors on the tangential component estimate may not give rise to errors of the magnitudes which were observed for the radial component. These errors are compounded by the fact that more than one beam of data is required to calculate the vector component estimate. Since the effect of this type of error on the estimate from the vector current algorithm is not known, a simulation is presented which illustrates the magnitudes of this kind of error. The algorithm parameters used

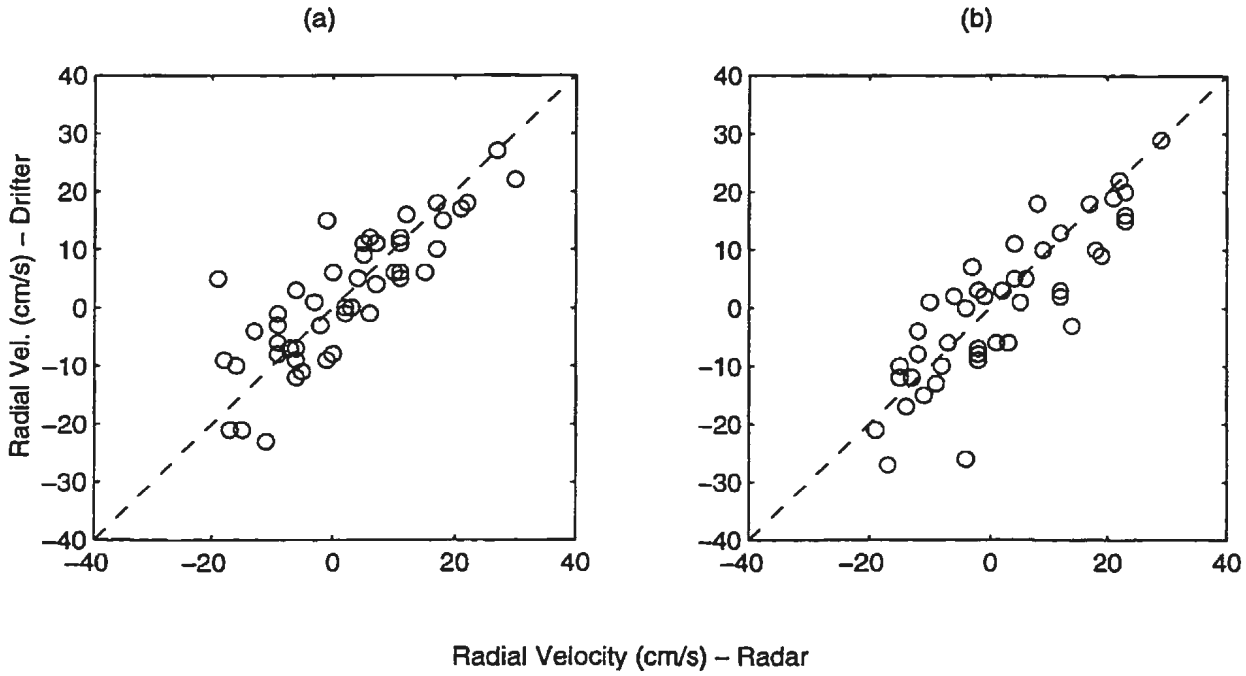

Figure 5.8: Scattergrams of direct radial component comparison using (a) the original radar data and (b) the beam-errored radar data. Note the similar scatter between the two sets.

in the simulation are equivalent to the parameters used in the case 1 study of Section 5.3. The input data is the simulated beam-errored data which was generated for the simulation description of the previous paragraph. The outputs from the simulation are the radial and tangential components estimated from the vector current algorithm. A comparison is shown in Figure 5.9 where the actual data case is compared to the simulated result. Even though the radial components are estimated to within reason for both cases, the tangential components exhibit significantly more variability. As illustrated by this example, it is plausible that beam direction errors may be responsible for the results observed in the actual tangential component comparison.

Another problem that may affect the radar/drifter comparison is that the current resolution of both measurement techniques may be too coarse for adequate sensing of the currents monitored in this experiment. In other words, the currents are difficult to measure with any precision since they are not significantly larger than the radar and

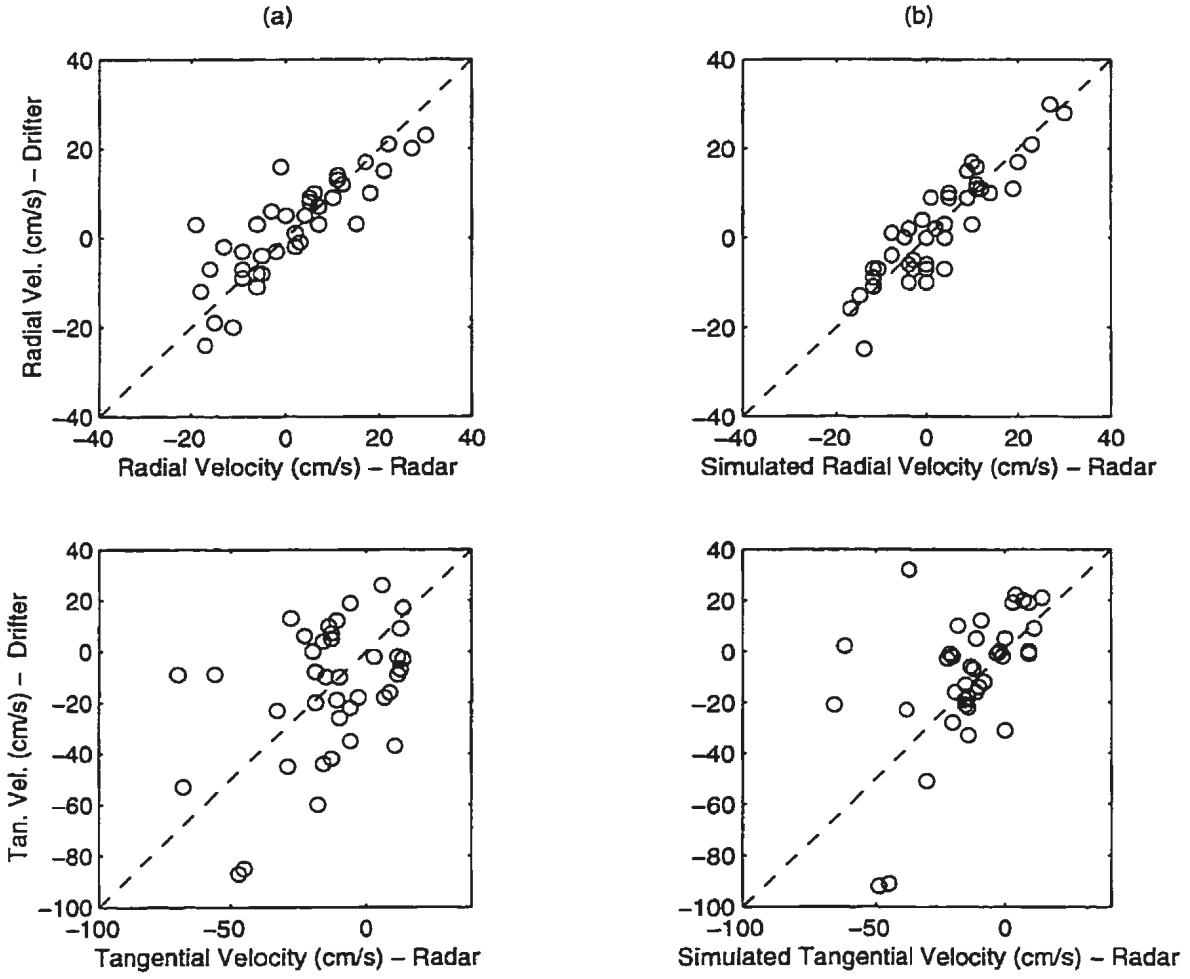

Figure 5.9: Scattergrams of vector component comparison using (a) the original radar data and (b) the beam-errored radar data. Note the increase in the variability of the tangential component estimates

drifter current errors. For example, from Table 5.2 it is observed that the standard deviations of the radial currents estimated by the radar and drifters throughout the experimental period, σ_x and σ_y, respectively, are approximately twice that of the regression error of the comparison, s. Therefore, since the current magnitudes are not significantly larger than the current velocity resolution of the radar system or the drifter error, conclusions regarding the quality of the radar direct radial current estimates may be premature. Moreover, when coupled with the above beamforming issue, it is not quite clear just how well the radar or drifters perform in monitoring

ocean surface currents where the current regime consists of currents which are not significantly larger than the sensor errors. It is evident that future experiments must be carefully planned when testing the current measuring capabilities of a HF radar system operating in the ground wave mode[4].

5.4 Discussion

The radial components estimated from the vector current algorithm, using simulated and actual data, strongly agree with the drifter computed estimates. The standard deviations are within the known errors of both techniques and the results are well correlated.

The radial components computed from the direct radar estimate and the estimate from the vector current algorithm correspond well with the drifter computed estimates. The standard deviations are within the known errors of both techniques and the results are well correlated.

Even though the tangential component estimates were highly correlated using simulated data, they were not very well correlated using the actual data with, at best, only 55% of the variability in the comparison explained by the regression. This may be due to extreme variability in the current field in the regions of interest (Petrie and Anderson [48]) or to beamforming errors. The latter possibility was discussed in the previous section. If beamforming problems did exist they were unknown during the experiment, with the exception of the major hardware problems noted during the later phases of the exercise. Since beam integrity is critical for the adequate testing

[4]Since the magnitudes of the errors of the radar estimated tangential current components indicate that the experimental radar data may be suspect, the inquiring reader may wonder why no other HF radar datasets were tested with the vector current processing scheme. HF radar data from two other current monitoring experiments are available from the Cape Race system. The first dataset was collected during the fall of 1991 to map and study the radial current patterns estimated by the radar. However, there was no sea-truthing made available for that exercise to provide data to test the vector current algorithm. The other dataset was collected in the fall of 1996. Even though sea-truthing drifters were deployed during that period, the azimuthal resolution of the radar data was too coarse to provide adequate test data for the algorithm.

of the vector current algorithm, further experiments should be performed and this parameter carefully monitored.

Chapter 6

Conclusions

6.1 Direct Radial Currents

The radial surface current components, estimated from the drifter tracks of three AST drifter buoys, were compared to those estimated from the first-order components of the spectra processed from data collected at the long-range HF facility at Cape Race, NF, during the fall of 1992. Each radar estimate was computed from the mean of all the radar current measurements that were within a circle of radius 2.5 km centred about the position of each drifter estimate. The standard deviation of the drifter and radar estimates were approximately 6 and 4 cm/s, respectively. This comparison produced standard deviations between the two which were within the error bounds of both techniques, or approximately 6.5 cm/s using a linear regression analysis. This was also demonstrated with simulations, albeit with a slightly smaller error of approximately 6 cm/s.

The following points are also noteworthy from the analysis:

- A 10 dB SNR for the Bragg components of the Doppler spectra has been shown to be sufficient for day-time radar operation;
- The standard error of the radar estimate does not exhibit any dependency on range or azimuth; and
- The results were shown to be independent of the sea state conditions witnessed

during the trial period, where wind speeds from 10 - 90 km/hour were experienced.

6.2 Vector Currents

Currents were assumed to be uniform over three polar extents, each spanned in the radial direction by 4.8 km and in azimuth by 12°, 20° and 36°, respectively. The radar components estimated from all three cases were compared to the drifter estimated components from one AST buoy. Using simulated and actual radar data for these cases, the results demonstrate the algorithm can estimate the radial current components to within 7 cm/s, or approximately within one standard deviation of both techniques. The result for the radial component case may be independent of the azimuthal extent since the correlation coefficients were not significantly different for all three cases. However, this may also be due to mean radial components in the regions that exhibited little relative variability.

The tangential component errors for the simulations were well behaved, exhibiting a nominal standard error of approximately 6 cm/s. However, for the actual data the errors were too large to consider the results useful for the cases examined. This may be due to non-uniform currents, non-stationary currents over the beam switching interval, as mentioned in Section 4.3, or possible sensor resolution and beamforming problems which were discussed in Section 5.3. The standard deviations from the actual data results indicate the tangential component error to be approximately 2.5 times the radial component error, or approximately 18 cm/s. However, since the simulations produced a more reasonable error of approximately 7 cm/s, the additional error may be due to the above mentioned anomalies and their sources, which were discussed in Section 5.3.2.2. These will have to be addressed in future studies using a more controlled experiment.

Though convincing results using actual data were not obtained for the radar tan-

gential component estimate, even with the observed errors the technique may still be useful for the estimation of the mean tangential component over large regions. The results for the cases considered produced a large relative error, but it is apparent from the scattergrams and the correlation coefficients that the statistical results indicate a better fit as the azimuthal extent is increased. Better results may certainly be obtained if the outstanding issues mentioned in the above paragraph were resolved. However, the validity of this estimate may ultimately depend on the current variability in the region, which has not been considered here. If the technique can provide a mean current estimate capability for large oceanic sectors, it is still quite a useful result since this parameter can't be estimated, in real-time, by other systems.

In conclusion, because of the following unknowns:

- Degree of current uniformity about drifter estimate;
- Possible non-stationary currents within beam switching intervals; and
- Possible beamforming problems

the performance of the vector current algorithm has not been rigorously established. However, the simulations suggest this parameter can be easily estimated to within one standard deviation of the drifter and radar velocity distributions under uniform current conditions.

6.3 Discussion

Since the vector current algorithm senses the radial current change over azimuth to estimate the other orthogonal current component, the extent of this azimuth in relation to the radar beamwidth is an important parameter. Obviously, this extent should reflect the extent of the uniform current region. Clearly then, as this extent decreases, the radar performance is dependent on the 'narrowness' of the receiving

beam for spatial selectivity. Optimally, each beam synthesized by the radar should isolate a different radar scattering area, or 'pie-piece' from the radar coverage zone such that the number of adjacent beams, and hence the region size, is kept to a minimum. If the extent is too large, the risk of using current data from a non-uniform region increases.

The resolving power of any radar system is dependent on its ability to distinguish between multiple targets within a radar scattering cell. However, for currents there is only one fundamental target, that being ocean waves that are matched to the radar carrier via the Bragg phenomenon. The mean current is indirectly sensed by this mechanism for each radar cell. Therefore, the cell size is a measure of the spatial resolution of a current measuring HF radar. Since the sector used for vector current estimation consists of a number of these cells, from a least squares perspective, as this number increases better estimates of the mean current may be expected. Further, the size of this number is a function of the radar system parameters such as antenna beamwidth and radar bandwidth, which define the arc and radial extents, respectively, of the cell. Therefore, in the design phase of a current measuring radar system, these parameters must be carefully selected, based on the knowledge of the current regimes which are to be monitored.

For the estimation of vector currents at long ranges it is necessary to synthesize very narrow beams. This may not be practical at coastal sites because at HF they require antenna arrays which are hundreds of meters in length. Hence, for a practical system, if the beamwidth is not adequate to estimate fine scale current measurements at long ranges it may be necessary to provide a second station to sense the current field from another direction. However, if a fine-resolution one-station system, which overcomes the aperture limitations of a linear array, can be developed, the method presented here may provide a framework for a practical real-time current monitoring system.

One of the goals of this thesis has been to illustrate the potential of using a single-station radar to estimate both radial and tangential current components. This is certainly possible as the simulations have demonstrated. However, further studies will need to be attempted, with more extensive simulations and groundtruthing exercises to validate the technique with actual data.

Even though the technique developed here may not duplicate the accuracy obtained from a two-site system it may still be sufficient for search and rescue purposes, or for oil spill contingency planning where gross surface transport may be required as opposed to fine-resolution point measurements.

6.4 Future Developments

The most important radar parameter for the estimation of ocean currents is the Doppler frequency resolution of the system, since this dictates the resolving power of the radar with respect to current magnitude detection. To improve on this resolution the examination of modern spectral estimation techniques may have to be considered (Hickey *et al.* [54]). These techniques may be used to obtain a better estimate of the displaced Bragg frequencies and hence the radial current. Such techniques usually require fewer samples than the FFT power spectral estimate, thereby allowing a scan of the radar coverage area to be performed in a more timely manner than presently possible. For example, a full scan of the coverage area requires approximately one hour of data collection to yield the velocity resolution provided by the experimental data presented here. If only 32 time samples for each beam were required, as opposed to 512 to obtain a spectral estimate, the same zone could be scanned in approximately 10 minutes. This is very advantageous, especially in the area of search and rescue or oil-spill tracking, where timely and regular surface current updates are required. It is also important for single-station vector current estimation since the sea is more likely to remain stationary from beam to beam, with respect to its statistical properties,

as this scan time is reduced.

Other algorithms may be evaluated for total current vectors, such as those using the equation of continuity (Frisch and Leise [55]). In addition, these may be incorporated into the present algorithm as constraints or as additional variables in a least squares approach to the solution.

Another approach to the solution could be attempted by using an iterative technique. It has been shown that the radial component can be calculated directly from the radar data. However, by varying the tangential component in the formulations developed in Chapter 2, a tangential estimate which minimizes the error, with respect to the known constraints on the radial component, may be computed. This could lead to another estimate of the tangential component. In the present formulation the regression approach reduces the overall error, thus neglecting the mean known radial component.

The quality of the measured ocean surface parameters has to be of prime importance. A level of confidence has to be assigned to each estimate such that a user can quantify the error in the result. Statistical techniques must be incorporated in the radar measurements such that the user has some degree of certainty in the measured quantity. The uncertainties should propagate throughout the analysis, from the initial antenna voltages to the resultant current maps. Since the parameters to be estimated are random variables with known statistics, techniques which are available to quantify these errors should be used (Lipa and Barrick [17]).

Future experiments must ensure that beam integrity is preserved, such that errors incurred here are within some angular tolerance level. This level should be a function of the error in the spectral estimator used to calculate the Bragg frequencies. This is especially important if finer resolution radial current measurements are made, since the correlation between adjacent beam directions should be kept to a minimum to enhance spatial selectivity.

Future work will also deal with the fine tuning of the vector current technique presented here, via modern statistical procedures. The simple analysis procedure used here may be adequate for demonstration purposes but a more robust solution must be devised and areas to be examined may include, but are not limited to, residual analysis, detection and treatment of outliers, refined model fitting, and weighted least squares solutions (Montgomery and Peck [53]).

The subject of the vorticity of the current field has not been addressed here. For example, "can eddy currents be extracted using the method or some variation of the method presented here?" In other words, "will the fundamentals of the algorithm permit the estimation of a non-uniform field where the radial components are constant but small, across many beams?" A minimum capability, with respect to radar performance, would be the identification of the location of these current features.

More extensive simulations should be used to study the effect of system parameters. For example, the fundamental waveform used by the radar should be properly simulated such that variations in the Bragg frequency from cell to cell may be better understood. In this study the Bragg frequency was assumed to be the centre frequency of the transmission band. However, this oversimplifies what may be actually occurring since the radar bandwidth was actually 375 kHz. Beam pattern simulations should also be incorporated so as to study the effect of side lobes, which may contaminate the data when the predominant wind direction coincides with one of these lobes.

To test the algorithm for the estimation of the mean current field an experiment should be devised to deploy many closely-spaced drifters, such that the actual mean current can be estimated. A positive result in this case may still be useful for the estimation of temporal meso-scale current variations.

References

[1] D. Barrick, "Remote sensing of sea state by radar," in *Remote Sensing of the Troposphere* (V. Derr, ed.), ch. 12, pp. 1–46, Washington, DC: U.S. Government Printing Office, 1972.

[2] J. Walsh and R. Donnelly, "A consolidated approach to two-body electromagnetic scattering problems," *Phys. Review A*, vol. 36, no. 9, pp. 4474–4485, 1987.

[3] J. Walsh, R. Howell, and B. Dawe, "Model development for evaluation studies of ground wave radar," Contract Report 90-C14, Centre for Cold Ocean Resources Engineering, 1990. Prepared for Department of National Defence, Government of Canada, DSS Contract Number W7714-8-5655/01-SS.

[4] K. Hickey and R. Khan, "Results of the 1991 CODAR surface current experiment," Contract Report 92-C9, Department of Supply and Services, 1992.

[5] R. Howell and J. Walsh, "Measurement of ocean wave spectra using narrow beam HF radar," *IEEE J. Oceanic Eng.*, vol. 18, no. 3, pp. 296–305, 1993.

[6] E. Gill and J. Walsh, "Extraction of ocean wave parameters from HF backscatter received by a four-element array: Analysis and application," *IEEE J. Oceanic Eng.*, vol. 17, no. 4, pp. 376–386, 1992.

[7] D. Barrick, J. Headrick, R. Bogle, and D. Crombie, "Sea backscatter at HF: Interpretation and utilization of the echo," *Proceedings IEEE*, vol. 62, pp. 673–680, June 1974.

[8] R. Stewart and J. Joy, "HF radio measurements of surface currents," *Deep-Sea Research*, vol. 21, pp. 1039–1049, 1974.

[9] D. Hodgins, "Oceanographic information of the eastern canadian offshore," Data Report 82-3, Seaconsult Marine Research, St. John's, Newfoundland, 1984.

[10] R. Beardsley, J. Scott, and W. Boicourt, "CMICE 76: A current meter intercomparison experiment conducted off Long Island in February-March 1976," Technical Report 62, Woods Hole Oceanographic Institution, 1977.

[11] D. Halpern, *Air Sea Interaction.* New York: Plenum Pub. Co., 1980. M. Kline (ed.).

[12] R. Weller and R. Davis, "A vector-measuring current meter," *Deep Sea Res.*, vol. 27, pp. 565–582, 1980.

[13] P. E. Smith, "An intercomparison of near-surface measurements with Aanderaa and AMF VACM current meters in strong tidal currents," Data Report 82-3, Department of Fisheries and Oceans, Ocean Science and Surveys Atlantic, Bedford Institute of Oceanography, 1984.

[14] D. Diemand, E. Riemer, and J. Barrie, "Ocean drifter studies of surface currents along the coasts of Newfoundland and Labrador and in the Beaufort Sea," Data Report 82-3, Centre for Cold Ocean Resources Engineering, St. John's, Newfoundland, 1982.

[15] B. Petrie and A. Isenor, "An analysis of satellite-tracked drifter observations collected in the grand banks region," Tech. Rep. 39, Canadian Technical Report of Hydrography and Ocean Sciences, 1984.

[16] D. Crombie, "Doppler spectrum of sea echo at 13.56 Mc./s.," *Nature*, vol. 175, pp. 681–682, 1955.

[17] B. Lipa and D. Barrick, "Least-squares methods for the extraction of surface currents from CODAR crossed-loop data: Application at ARSLOE," *IEEE J. Oceanic Eng.*, vol. 8, no. 4, pp. 226–253, 1983.

[18] D. Prandle and D. Ryder, "Measurement of surface currents in Liverpool Bay by High-Frequency radar," *Nature*, vol. 315, pp. 128–131, 1985.

[19] M. Janopaul, J. P. Broche, Maistre, H. Essen, C. Blanchet, G. Grau, and E. Mittelstaedt, "Comparison of measurements of sea currents by HF radar and conventional means," *Int. J. of Remote Sensing*, vol. 3, pp. 409–422, 1982.

[20] R. P. Dinsmore, "Ice and its drift into the North Atlantic Ocean," in *I.C.N.A.F Spec. Publ. No. 8. Symp. on Environmental conditions in the Northwest Atlantic*, (Dartmouth, N.S.), 1972.

[21] J. Wait, "Concerning the theory of scatter of HF radio ground waves," in *Electromagnetic Probing in Geophysics* (J. Wait, ed.), Boulder, Colorado: Golem Press, 1971.

[22] J. Wait, "Theory of HF ground wave backscatter from sea waves," *J. Geophys. Res.*, vol. 71, no. 20, pp. 4839–4842, 1966.

[23] W. H. Peake, "Theory of radar return from terrain," in *1959 IRE Int. Conv. Rec.*, pp. 27–41, 1959.

[24] S. Rice, *Reflection of electromagnetic waves from slightly rough surfaces.* New York: New York:Interscience, 1950.

[25] D. Crombie, "Backscatter of HF radio waves from the sea," *Electromagnetic Probing in Geophysics*, pp. 131–162, 1971. J.R. Wait (ed.).

[26] D. Crombie, "Resonant backscatter from the sea and its application to physical oceanography," in *Oceans '72 Conf. Rec.*, pp. 173–179, IEEE Publ. No. 72CHO 660-1 OCC, 1972.

[27] J. Wu, "Wind-induced drift currents," *J. Fluid Mech.*, vol. 68, pp. 49–70, 1975.

[28] W. H. Munk, G. Miller, F. Snodgrass, and N. Barber, "Directional recording of swell from distant storms," *Phil. Trans. Roy. Soc.*, vol. 255, no. 1062, 1963.

[29] J. Holbrook and A. Frisch, "A comparison of near-surface CODAR and VACM measurements in the Strait of Juan de Fuca," *J. Geophys. Res.*, vol. 86, pp. 10908–10912, 1981.

[30] D. Lawrence and P. Smith, "Evaluation of HF ground-wave radar on the east coast of Canada," *IEEE J. Oceanic Eng.*, vol. 11, no. 2, pp. 246–250, 1986.

[31] D. Hodgins, "Evaluation of the coastal ocean dynamics radar for surface current measurement," contract report, Seaconsult Marine Research, Vancouver, B.C., 1989.

[32] P. G. Collar., D. Eccles, M. J. Howarth, and N. Millard, "An intercomparison of HF radar observations of surface currents with moored current meter data and displacement rates of acoustically tracked droqued floats," in *Fourth Ocean Data Conference, Society for Underwater Technology*, (London, Eng.,), 1985.

[33] J. F. Venn, G. T. Mardell, J. Howarth, and C. G. Holmes, "Current measurement by long range HF ground-wave radar," in *Proc. of IGARSS '88 Symposium*, (Edinburgh, Scotland), 1988.

[34] H. Essen, E. Mittelstaedt, and F. Schirmer, "On near-shore surface current measurement by means of radar," *Dtsch. Hydrogr. Z.*, vol. 34, pp. 1–14, 1981.

[35] D. Prandle, "Measuring currents at the sea surface by HF radar (OSCR)," *J. of the Soc. for Underwater Technology*, vol. 11, pp. 24–27, 1985.

[36] M. Heron, P. Dexter, and B. Mcgann, "Parameters of the air-sea interface by high-frequency ground-wave HF Doppler radar," *Aust. J. Mar. Freshw. Res.*, vol. 36, pp. 655–670, 1985.

[37] K. Butt, P. Jeans, and K. Hickey, "HF radar technology transfer project- implementation and testing of a two-site capability," Contract Report 83-11, Centre for Cold Ocean Resources Engineering, St. John's, Newfoundland, 1983.

[38] K. Butt and K. Hickey, "HF radar technology transfer project- single site data analysis," Contract Report 83-9, Centre for Cold Ocean Resources Engineering, St. John's, Newfoundland, 1983.

[39] J. Walsh, B. Dawe, and S. Srivastava, "Remote sensing of icebergs by ground wave doppler radar," *IEEE J. Oceanic Eng.*, vol. OE, no. 11, pp. 276–284, 1986.

[40] J. Walsh and S. Srivastava, "Rough surface propagation and scatter with applications to ground wave remote sensing in an ocean environment," in *Proc. AGARD (NATO) 40th EPP Specialist meeting, Rome, Italy*, pp. 23.1–23.15, 1987.

[41] B. Briggs, G. Phillips, and D. Shinn, "The analysis of observations on spaced receivers of the fading of radio waves," *Proc. Roy. Soc. London*, vol. B63, pp. 106–121, 1950.

[42] P. May, "Single station ocean current vector measurement :application of the spaced antenna (SA) technique," *Geophys. Res. Letters*, vol. 16, no. 9, pp. 999–1002, 1989.

[43] N. Levanon, *Radar Principles.* New York: John Wiley and Sons, 1988.

[44] R. Collin, *Antenna and Radiowave Propagation.* New York: McGraw-Hill, INc., 1985.

[45] R. Khan, B. Gamberg, D. Power, J. Walsh, B. Dawe, W. Pearson, and D. Millan, "Target detection and tracking with a high frequency ground wave radar," *IEEE J. Oceanic Eng.*, vol. 19, pp. 540–548, October 1994.

[46] D. Barrick, M. Evans, and B. Weber, "Ocean surface currents mapped by radar," *Science*, vol. 198, pp. 139–144, 1977.

[47] C. Anderson and R. Shaw, "The Canadian Atlantic Storms Project (CASP): an overview," in *Proc. of the International Workshop on Wave Hindcasting and Forecasting*, (Halifax, NS), pp. 3–13, ESRF, 1987.

[48] B. Petrie and C. Anderson, "Circulation on the Newfoundland continental shelf," *Atmosphere-Ocean*, vol. 21, no. 2, pp. 201–226, 1983.

[49] J. Helbig, "On the use of splines for extracting velocities from drifting buoy tracks," *J. Atmospheric Oceanic technol.*, vol. 229, pp. 16–17, 1994.

[50] R. Davis, "Beam forming for forty element HF groundwave radar antenna," in *Proc. NECEC 90, St. John's, NF, CA*, May 1990.

[51] D. Barrick and J. Snider, "The statistics of HF sea-echo doppler spectra," *IEEE Trans. Antennas Propagat.*, vol. AP-25, pp. 19–28, 1977.

[52] B. Lipa and D. Barrick, "Extraction of sea state from HF radar sea echo: Mathematical theory and modeling," *Radio Science*, vol. 21, no. 1, pp. 81–100, 1986.

[53] D. Montgomery and E. Peck, *Introduction to Linear Regression analysis.* New York: John Wiley and Sons, 1982.

[54] K. Hickey, R. Khan, and J. Walsh, "Parametric estimation of ocean surface currents with HF radar," *IEEE J. Oceanic Eng.*, vol. 20, April 1995.

[55] A. Frisch and J. Leise, "A note on using continuity to extend HF radar surface-current measurements," *J. Geophys. Res.*, vol. 86, pp. 11089–11090, 1981.

Appendix A

Chronology of the Experiment

DATE	TIME (LOCAL)	EVENT	Comments
21/10/92	10:00	Data collection begins	
	10:05	Hardware problem	Transmitter 'tripped'. This occurred after I deleted the data collection process from the queue and re-submitted it.
	10:50	Hardware problem corrected	The transmitter is fine now, for no apparent reason.
	11:55	Software problem #1	Array processing version of interpretation software failed due to a 'divide by zero' error at line 212 of the main program. Will use the Vax software until the problem can be found.
	13:00	Software problem #2	Raw Data file only contains 32 time series points for the first hardware beam. There must be an error in the data collection software as a result of recent changes in this module to accomodate this experiment. Raw data will be backed up anyway.

DATE	TIME (LOCAL)	EVENT	Comments
	17:30	Software problem #2 corrected	The backed up raw data can probably be re-processed at the end of the experiment.
21/10/92	21:00	System change	The radar frequency has been changed from 6.25 to 6.95 MHZ. There was a significant amount of interference at the other frequency.
22/10/92	10:10	System change	Operating at 6.95 MHz.
	15:00	System problem	Unusual periodicity noted in spectral data. This may not effect the current processing capability of the system but as a precautionary measure the operating frequency will be changed back to 6.25 MHz.
	20:00	System problem corrected	Operating frequency changed back to 6.25 MHz. Spectral periodicity has disappeared.
	23:00	System problem	A 'bug' found in data collection software. Yesterday's processed data may be affected. The periodicity of the spectral data noted at 15:00 today may be caused by this.
23/10/92	14:00	Processing Error	Processed data starts at 76 km instead of 44. This effects data file CUR_RAD_29692.001 and ...002. As a result, one of the 'drifters', at a range of 64 km, may not have been surveyed.

DATE	TIME (LOCAL)	EVENT	Comments
24/10/92	18:00	Software problem	Processed data files from data collected at 13:00 and 16:00 may be corrupt. Beam number 28 was used today for the first time, which resulted in an indexing problem that effects the directionality associated with the data.
28/10/92	09:30 10:30	Power down Power restored	Newfoundland Power working in Trepassey
30/10/92	16:00	Software problem	'Floating divide by zero' from VAX current software processing data file D3_1. Data collection and array processing software testing was performed during the same period. There may be a problem in using both array processors simultaneously.
04/11/92	09:40	Hardware problem	Transmitter 'tripped'.
	09:55	Hardware problem	Transmitter 'tripped' again. See problem of 21-Oct-92 as it occurred under the same circumstances. In the future, run NRSL$EXE:DEALLOCATE_ALL_SFTW to prevent this problem from occurring. It has something to do with the pre-processor not properly initializing itself upon system startup. This causes the transmitter malfunction.

DATE	TIME (LOCAL)	EVENT	Comments
04/11/92	21:00	Hardware change	Center frequency changed to 6.95 MHz for navy frigate trial.
05/11/92	12:00	Hardware change	Changed centre frequency back to 6.25, from 6.96 MHz. The inspected radial current velocity data displayed a variability which did not seem plausible.
	19:00	Hardware problem	Circuit breaker of second receiver rack had 'tripped'and this resulted in 5 missing channels of data. This may have affected the 16:50 data run today.
06/11/92	09:00	System down	Power down in Trepassey
	12:30	System up	Power up again
	20:30	Hardware problem	Channel #10 data may be corrupt. Its effects may not be very dramatic.
07/11/92	16:54	Hardware problem corrected	Channel #10 appears to be O.K. now.
12/11/92	18:00	Hardware change	Frequency changed to 6.95 MHz. There was too much interference at 6.25 MHz.

Appendix B

NRSL Current Velocity Data Tapes

Each data tape consists of radial velocity data processed from time series collected at Cape Race, NF, during the period Oct. 21 to Nov. 20, 1992. The processing was performed on a DEC Vax 8530 with VMS V5.1 and FORTRAN V5.5-98.

B.0.1 Tape Format

Each file on the tape is identified by the following literal:

CUR_RAD_MMMNN.PPP

where

MMMNN - a 5 digit integer indicating the Julian date of the data collection

where

MMM - Julian day

NN - Year

PPP - a 3 digit integer indicating the dataset number for the day.

For example, the file CUR_RAD_31992.004 contains data processed from the 4^{th} data set collected on the 319^{th} day of 1992.

The tape was created by using the DEC utility BACKUP.

The following examples will illustrate how the radial surface current data is retrieved from a magnetic tape using the VMS operating system.

Example: Retrieval of all the current data on tape.

```
$ ALL MUA0:
$ MOU MUA0:/FOR
$ BACKUP MUA0:JAN131992.BCK/LABEL=CUR  *.*
```

Example: Retrieve a subset of the data on tape.

```
$ ALL MUA0:
$ MOU MUA0:/FOR
$ BACKUP MUA0:JAN131991.BCK/LABEL=CUR/SELECT=[. . .]
CUR_RAD_31992.003    *.*
```

B.0.2 File format

Each file is of a *direct access* type containing NRANG×2+1 unformatted records where NRANG is the number of 400 meter processed range rings. Each record (except the header) consists of NANG REAL*4 values corresponding to NANG degrees of azimuth. The structure of this file is shown in figure B.1.

B.0.3 Reading The File

The following standard FORTRAN code can be used to access the data.

```
      OPEN(UNIT=LUN,TYPE='OLD',NAME='CUR_RAD_31992.001',ACCESS='DIREC'
+FORM='UNFORMATTED')
      READ (LUN,1)DATLOG,BORSIT,RANGE,NANG,NFFT,NFIELD,L_BEAR
```

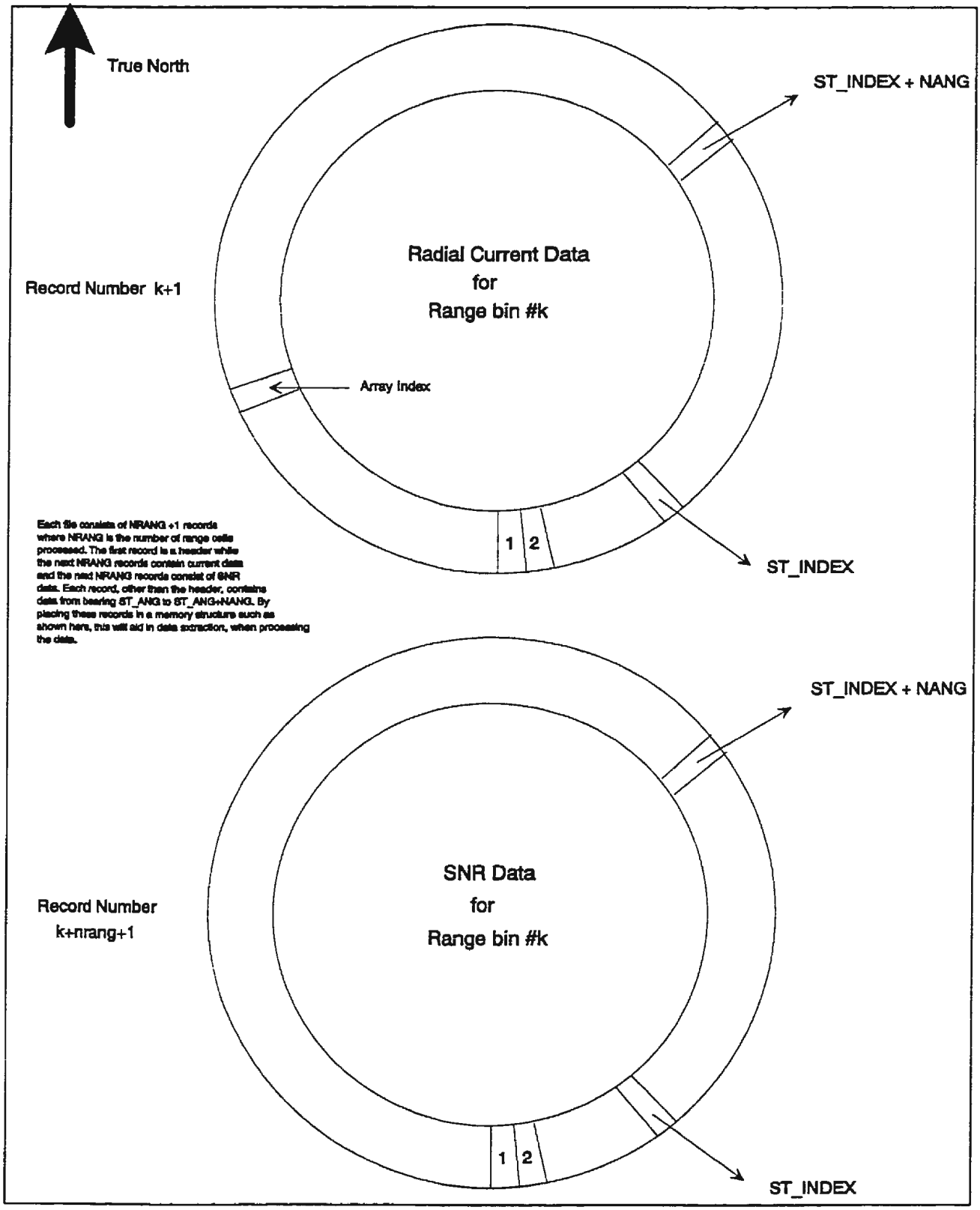

Figure B.1: Record structure for binary radial current files. Each record has a capacity for a full 360 degrees of azimuth where the index in the record references the azimuth

Where

DATLOG - Array of 32×3 bytes representing run logistic information such as site location and time of data collection

BORSIT - Receive antenna boresite is 'BORSIT' degrees clockwise from True North.(REAL*4)

RANGE - Array of 3 (4-byte) real values

where

RANGE(1) - Distance to middle of first range annulus (km)

RANGE(2) - Distance to middle of last range annulus (km)

RANGE(3) - Range annulus width (km)

NFFT - FFT size used to generate file (INTEGER*4)

NFIELD - Number of fields in data file format. For this data set NFIELD=2 (one for the radial velocities estimates and one for the SNR values). (INTEGER*4)

L_BEAR - The last bearing processed. This bearing indicates where the processed data begins . i.e. RAD(1) is from bearing L_BEAR, RAD(2) is from bearing L_BEAR+1, RAD(3) is from bearing L_BEAR+2, etc.

Each remaining record can be accessed as shown in the following example.

Let

NRANG - Number of range annulli processed

NANG - Number of angular bins (max. of 360)

RAD(360,NRANG) - (Real*4) array of radial velocity values

SNR(360,NRANG) - ...and their SNR values.

The Fortran code is as follows:

```
ST_ANG=-L_BEAR+180
ST_INDEX=MAX(1,MIN(ST_ANG,360))
DO IRANG=1,NRANG
  IREC=IRANG+1
  READ(LUN 'IREC)(RAD(I,IRANG),I=ST_INDEX,ST_INDEX+NANG)
  IREC=IRANG+NRANG+1
  READ(LUN 'IREC)(SNR(I,IRANG),I=ST_INDEX,ST_INDEX+NANG)
END DO
```

Notes:

By the way, NRANG = (RANGE(2)-RANGE(1))/RANGE(3).

The variable BORSIT may not be correct in the data file header. It should be the value 121. In any case, it doesn't matter what value is there. The proper boresite value is incorporated in the data record structure.

Appendix C

Catalogue of the NRSL Radial Surface Current Data

Date (1992)	Time (Local)	Filename CUR_RAD_	Starting range (km)	Ending range (km)	Initial Bearing °(True)	Final Bearing °(True)	FFT size
21/10	11:53	29492.001	10.4	300.4	60	155	512
22/10	10:10	29592.001	50.4	200.4	96	165	512
	14:17	29592.002	50.4	200.4	84	165	512
23/10	10:16	29692.001	76.0	170.4	104	176	512
	13:08	29692.002	76.0	170.4	104	176	512
	15:54	29692.003	44.4	170.4	104	176	512
	20:47	29692.004	12.0	152.4	104	176	512
24/10	10:31	29792.001	52.0	173.2	104	176	512
25/10	11:12	29892.001	40.0	241.2	95	180	512
	15:18	29892.002	44.0	170.4	104	180	512
26/10	10:24	29992.001	40.0	161.2	104	180	512
	13:00	29992.002	40.0	161.2	104	180	512
	17:44	29992.003	40.0	161.2	104	180	512
27/10	09:31	30092.001	40.0	161.2	104	180	512
	10:47	30092.002	40.0	199.6	94	165	512
28/10	10:40	30192.001	40.0	161.2	95	176	512
	13:31	30192.002	40.0	199.6	95	176	512
29/10	09:00	30292.001	40.0	161.2	95	176	512
	13:09	30292.002	80.0	220.4	95	176	512
30/10	09:30	30392.001	40.0	151.6	77	118	512
	12:00	30392.002	80.0	151.6	104	176	512
	16:06	30392.003	40.0	279.6	56	176	512

Date (1992)	Time (Local)	Filename CUR_RAD_	Starting range (km)	Ending range (km)	Initial Bearing °(True)	Final Bearing °(True)	FFT size
31/10	10:16	30492.001	60.0	162.0	104	176	512
	12:01	30492.002	60.0	162.0	104	180	512
	15:00	30492.003	60.0	162.0	104	180	512
01/11	09:24	30592.001	70.0	172.0	104	180	512
	12:00	30592.002	70.0	172.0	104	180	512
	15:00	30592.003	70.0	172.0	104	180	512
02/11	09:20	30692.001	80.0	159.6	104	180	512
	12:00	30692.002	80.0	159.6	104	180	512
	15:00	30692.003	80.0	159.6	104	180	512
03/11	09:39	30792.001	80.0	159.6	104	180	512
	12:00	30792.002	80.0	159.6	104	180	512
	15:01	30792.003	80.0	159.6	104	180	512
	16:36	30792.004	80.0	159.6	104	180	512
04/11	10:06	30892.001	100.0	179.6	138	179	512
	12:00	30892.002	100.0	179.6	138	179	512
	15:00	30892.003	100.0	179.6	138	179	512
	18:07	30892.004	100.0	179.6	138	176	512
05/11	10:38	30992.001	80.0	182.0	138	179	512
	15:23	30992.002	100.0	221.2	138	179	512
	16:49	30992.003	100.0	221.2	138	179	512
06/11	12:51	31092.001	100.0	221.2	138	179	512
	14:00	31092.002	80.0	182.0	135	176	1024
	15:39	31092.003	80.0	182.0	138	179	1024
07/11	10:05	31192.001	80.0	220.4	134	179	512
	12:00	31192.002	80.0	220.4	134	179	512
	15:00	31192.003	80.0	220.4	103	144	512
	18:00	31192.004	80.0	220.4	103	144	512
08/11	09:00	31292.001	80.0	220.4	105	169	512
	12:00	31292.002	80.0	220.4	105	169	512
	15:00	31292.003	80.0	220.4	105	179	512
	18:00	31292.004	80.0	220.4	105	179	512
09/11	10:05	31392.001	80.0	220.4	105	179	512
	12:00	31392.002	80.0	220.4	105	179	512
	15:01	31392.003	80.0	220.4	105	179	512
	18:00	31392.004	80.0	220.4	105	179	512
10/11	09:00	31492.001	80.0	220.4	105	179	512
	12:00	31492.002	100.0	240.4	105	179	512
	15:00	31492.003	80.0	239.6	64	180	512

Date (1992)	Time (Local)	Filename CUR_RAD_	Starting range (km)	Ending range (km)	Initial Bearing °(True)	Final Bearing °(True)	FFT size
11/11	09:00	31592.001	80.0	239.6	64	180	512
	10:38	31592.002	100.0	240.4	104	176	512
	12:00	31592.003	80.0	239.6	104	176	512
	15:00	31592.004	80.0	239.6	105	179	512
12/11	09:00	31692.001	80.0	239.6	105	179	512
	12:00	31692.002	120.0	260.4	105	179	512
	18:30	31692.003	80.0	239.6	105	179	512
13/11	09:00	31792.001	80.0	239.6	105	179	512
	12:00	31792.002	120.0	260.4	105	179	512
	15:00	31792.003	80.0	239.6	105	179	512
	18:00	31792.004	80.0	239.6	105	179	512
14/11	09:00	31892.001	80.0	239.6	105	179	512
	12:00	31892.002	120.0	260.4	105	179	512
	14:43	31892.003	10.4	203.6	57	176	512
	17:23	31892.004	80.0	239.6	105	179	512
15/11	09:00	31992.001	80.0	239.6	105	179	512
	12:00	31992.002	120.0	260.4	105	179	512
	15:00	31992.003	80.0	239.6	105	179	512
	18:00	31992.004	80.0	239.6	105	179	512
16/11	09:31	32092.001	80.0	239.6	105	179	512
	12:00	32092.002	120.0	260.4	105	179	512
	15:00	32092.003	80.0	239.6	105	179	512
	18:00	32092.004	80.0	239.6	105	179	512
17/11	09:00	32192.001	80.0	239.6	105	179	512
	12:00	32192.002	120.0	260.4	105	179	512
	15:00	32192.003	80.0	239.6	105	179	512
	18:00	32192.004	80.0	239.6	105	179	512
18/11	06:00	32292.001	80.0	239.6	105	179	512
	09:00	32292.002	120.0	260.4	105	179	512
	12:00	32292.003	80.0	239.6	105	179	512
	15:00	32292.004	80.0	239.6	105	179	512
19/11	09:33	32392.001	80.0	239.6	105	179	512
	12:00	32392.002	120.0	260.4	105	179	512
	15:00	32392.003	80.0	239.6	105	179	512
20/11	07:00	32492.001	80.0	239.6	105	179	512
	10:00	32492.002	80.0	239.6	105	179	512
	13:00	32492.003	120.0	260.4	105	179	512

Appendix D

Cross-Reference Table for Radial Surface Current Data

Date	Time (Local)	Filename	FFT size
21/10/92	11:53	CUR_RAD_29492.001	512
22/10/92	10:10	CURRAD29592.001	512
	14:17	CURRAD29592.002	512
23/10/92	10:16	CURRAD29692.001	512
	13:08	CURRAD29692.002	512
	15:54	CURRAD29692.003	512
	20:47	CURRAD29692.004	512
24/10/92	10:31	CURRAD29792.001	512
25/10/92	11:12	CURRAD29892.001	512
	15:18	CURRAD29892.002	512
26/10/92	10:24	CURRAD29992.001	512
	13:00	CURRAD29992.002	512
	17:44	CURRAD29992.003	512
27/10/92	09:31	CURRAD30092.001	512
	10:47	CURRAD30092.002	512
28/10/92	10:40	CURRAD30192.001	512
	13:31	CURRAD30192.002	512
29/10/92	09:00	CURRAD30292.001	512
	13:09	CURRAD30292.002	512
30/10/92	09:30	CURRAD30392.001	512
	12:00	CURRAD30392.002	512
	16:06	CURRAD30392.003	512
31/10/92	10:16	CURRAD30492.001	512
	12:01	CURRAD30492.002	512
	15:00	CURRAD30492.003	512

Date	Time (Local)	Filename	FFT size
01/11/92	09:24	CURRAD30592.001	512
	12:00	CURRAD30592.002	512
	15:00	CURRAD30592.003	512
02/11/92	09:20	CURRAD30692.001	512
	12:00	CURRAD30692.002	512
	15:00	CURRAD30692.003	512
03/11/92	09:39	CURRAD30792.001	512
	12:00	CURRAD30792.002	512
	15:01	CURRAD30792.003	512
	16:36	CURRAD30792.004	512
04/11/92	10:06	CURRAD30892.001	1024
	12:00	CURRAD30892.002	1024
	15:00	CURRAD30892.003	1024
	18:07	CURRAD30892.004	1024
05/11/92	10:38	CURRAD30992.001	2048
	15:23	CURRAD30992.002	512
	16:49	CURRAD30992.003	512
06/11/92	12:51	CURRAD31092.001	512
	14:00	CURRAD31092.002	1024
	15:39	CURRAD31092.003	1024
07/11/92	10:05	CURRAD31192.001	512
	12:00	CURRAD31192.002	512
	15:00	CURRAD31192.003	512
	18:00	CURRAD31192.004	512
08/11/92	09:00	CURRAD31292.001	512
	12:00	CURRAD31292.002	512
	15:00	CURRAD31292.003	512
	18:00	CURRAD31292.004	512
09/11/92	10:05	CURRAD31392.001	512
	12:00	CURRAD31392.002	512
	15:01	CURRAD31392.003	512
	18:00	CURRAD31392.004	512
10/11/92	09:00	CURRAD31492.001	512
	12:00	CURRAD31492.002	512
	15:00	CURRAD31492.003	512
11/11/92	09:00	CURRAD31592.001	512
	10:38	CURRAD31592.002	512
	12:00	CURRAD31592.003	512
	15:00	CURRAD31592.004	512

Date	Time (Local)	Filename	FFT size
12/11/92	09:00	CURRAD31692.001	512
	12:00	CURRAD31692.002	512
	18:30	CURRAD31692.003	512
13/11/92	09:00	CURRAD31792.001	512
	12:00	CURRAD31792.002	512
	15:00	CURRAD31792.003	512
	18:00	CURRAD31792.004	512
14/11/92	09:00	CURRAD31892.001	512
	12:00	CURRAD31892.002	512
	14:43	CURRAD31892.003	512
	17:23	CURRAD31892.004	512
15/11/92	09:00	CURRAD31992.001	512
	12:00	CURRAD31992.002	512
	15:00	CURRAD31992.003	512
	18:00	CURRAD31992.004	512
16/11/92	09:31	CURRAD32092.001	512
	12:00	CURRAD32092.002	512
	15:00	CURRAD32092.003	512
	18:00	CURRAD32092.004	512
17/11/92	09:00	CURRAD32192.001	512
	12:00	CURRAD32192.002	512
	15:00	CURRAD32192.003	512
	18:00	CURRAD32192.004	512
18/11/92	06:00	CURRAD32292.001	512
	09:00	CURRAD32292.002	512
	12:00	CURRAD32292.003	512
	15:00	CURRAD32292.004	512
19/11/92	09:33	CURRAD32392.001	512
	12:00	CURRAD32392.002	512
	15:00	CURRAD32392.003	512
20/11/92	07:00	CURRAD32492.001	512
	10:00	CURRAD32492.002	512
	13:00	CURRAD32492.003	512